Long noncoding RNA *ANRIL* regulates endothelial cell activities associated with coronary artery disease by up-regulating *CLIP1*, *EZR*, and *LYVE1* genes

Received for publication, July 25, 2018, and in revised form, January 11, 2019 Published, Papers in Press, January 17, 2019, DOI 10.1074/jbc.RA118.005050

Hyosuk Cho[‡§¶], Gong-Qing Shen[§¶1], Xiaofeng Wang[‖1], Fan Wang[§¶1], Stephen Archacki[§¶1], Yabo Li[§¶], Gang Yu[§¶], Susmita Chakrabarti[§¶], Qiuyun Chen[§¶2], and Qing Kenneth Wang[‡§¶**3]**

*From the [‡]Department of Genetics and Genome Sciences, Case Western Reserve University, Cleveland, Ohio 44106, the Departments of [§]Cardiovascular and Metabolic Sciences and [‖]Quantitative Health Sciences, Lerner Research Institute, Cleveland Clinic, Cleveland, Ohio 44195, the [¶]Department of Molecular Medicine, Cleveland Clinic Lerner College of Medicine of Case Western Reserve University, Cleveland, Ohio 44195, and the **Key Laboratory of Molecular Biophysics of the Ministry of Education, Cardio-X Center, College of Life Science and Technology and Center for Human Genome Research, Huazhong University of Science and Technology, Wuhan 430073, China*

Edited by Ronald C. Wek

Coronary artery disease (CAD) is the leading cause of death worldwide. Long noncoding RNAs (lncRNAs) are a class of noncoding transcripts of > 200 nucleotides and are increasingly recognized as playing functional roles in physiology and disease. *ANRIL* is an lncRNA gene mapped to the chromosome 9p21 genetic locus for CAD identified by the first series of genome-wide association studies (GWAS). However, *ANRIL*'s role in CAD and the underlying molecular mechanism are unknown. Here, we show that the major *ANRIL* transcript in endothelial cells (ECs) is *DQ485454* with a much higher expression level in ECs than in THP-1 monocytes. Of note, *DQ485454* expression was down-regulated in CAD coronary arteries compared with non-CAD arteries. DQ485454 overexpression significantly reduced monocyte adhesion to ECs, transendothelial monocyte migration (TEM), and EC migration, which are critical cellular processes involved in CAD initiation, whereas siRNA-mediated *ANRIL* knockdown (KD) had the opposite effect. Microarray and follow-up quantitative RT-PCR analyses revealed that the *ANRIL* KD down-regulated expression of *AHNAK2*, *CLIP1*, *CXCL11*, *ENC1*, *EZR*, *LYVE1*, *WASL*, and *TNFSF10* genes and up-regulated *TMEM100* and *TMEM106B* genes. Mechanistic studies disclosed that overexpression of *CLIP1*, *EZR*, and *LYVE1* reversed the effects of *ANRIL* KD on monocyte adhesion to ECs, TEM, and EC migration. These findings indicate that *ANRIL* regulates EC functions directly related to CAD, supporting the hypothesis that *ANRIL* is involved in CAD pathogenesis at the 9p21 genetic locus and identifying a molecular mechanism underlying lncRNA-mediated regulation of EC function and CAD development.

Coronary artery disease (CAD)[4] is the most common cardiovascular disease and the leading cause of death worldwide (1). It occurs as a chronic inflammatory response to endothelial injuries in coronary arteries. Then the coronary arteries develop an atherosclerotic plaque inside the intima (referred to as atherosclerosis), leading to hardening and narrowing of the arteries and blocking of blood flow to the heart. Typical CAD complications include stable angina, unstable angina, myocardial infarction (MI), arrhythmias, heart failure, and sudden death (2).

For the development of atherosclerosis and CAD, monocyte adhesion to the endothelium and transendothelial migration of monocytes (TEM) into the intima have been established as two of the most important cellular processes by multiple studies (1, 2). An increased serum concentration of oxidized low-density lipoproteins (ox-LDLs) or other inflammatory molecules such as TNFα recruits monocytes to the region where ROS-induced endothelial dysfunction occurs (1–3). This leads to monocyte adhesion to the endothelium, followed by transmigration of monocytes across the endothelium into the intima area (1–3). The monocytes are then transformed into lipid-engorged macrophages and foam cells, leading to the formation of plaques (1–3).

This study was supported by NHLBI, National Institutes of Health, Grants R01 HL121358 and R01 HL126729; American Heart Association Innovative Research Grant 11IRG5570046. The authors declare that they have no conflicts of interest with the contents of this article. The content is solely the responsibility of the authors and does not necessarily represent the official views of the National Institutes of Health.

This article contains Tables S1 and S2 and Figs. S1–S4.

The data discussed in this publication have been deposited in NCBI's Gene Expression Omnibus and are accessible through GEO Series accession number GSE117676.

[1] These authors contributed equally to this work.

[2] To whom correspondence may be addressed: Dept. of Cardiovascular and Metabolic Sciences, Lerner Research Institute, Cleveland Clinic, Cleveland, Ohio 44195. Tel.: 216–444-2122; Fax: 216–444-9263; E-mail: chenq3@ccf.org.

[3] To whom correspondence may be addressed: Dept. of Cardiovascular and Metabolic Sciences, Lerner Research Institute, Cleveland Clinic, Cleveland, Ohio 44195. Tel.: 216–444-2122; Fax: 216–444-9263; E-mail: wangq2@ccf.org.

[4] The abbreviations used are: CAD, coronary artery disease; MI, myocardial infarction; TEM, transendothelial monocyte migration; ox-LDL, oxidized low-density lipoprotein; GWAS, genome-wide association studies; lncRNA, long noncoding RNA; EC, endothelial cell; TNFα, tumor necrosis factor α; KD, knockdown; HCAEC, human coronary artery EC; HUVEC, human umbilical vascular EC; GO, gene ontology; IL, interleukin; FBS, fetal bovine serum; RMA, robust multi-array average; GAPDH, glyceraldehyde-3-phosphate dehydrogenase; qRT-PCR, quantitative RT-PCR; Cad, cadherin.

Genetic factors contribute significantly to the pathogenesis of CAD. GWAS have revolutionized the genetic studies of common complex diseases, including CAD, and are considered as the most effective genetic strategy for unbiased identification of novel genetic variants and loci associated with CAD and other common diseases (4). The first series of GWAS for CAD identified a novel CAD risk locus on chromosome 9p21.3 (4, 5). To date, the 9p21.3 locus is the most robust and frequently replicated risk locus of CAD among >90 CAD risk loci identified by GWAS (4–7). However, the causative gene for CAD at the 9p21.3 locus is unknown. Interestingly, the *ANRIL* gene (which was initially referred to as antisense non-coding RNA in INK4 locus and encodes a long noncoding RNA (lncRNA)) is located within the 9p21.3 CAD locus (6–8). More than 50 CAD-associated genomic variants were identified to be located at the 9p21.3 CAD locus, and many of them are located within *ANRIL*, which makes *ANRIL* a strong candidate gene for CAD at the locus (6–8).

The *ANRIL* gene encodes a 3.8-kb lncRNA, which consists of 19 exons, spans over 126 kb, and is highly expressed in endothelial cells (ECs) (4–11). Multiple studies with human tissue samples showed a reduced expression level of *ANRIL* in both white blood cells and coronary artery samples from CAD and MI patients compared with non-CAD controls (6, 8–11). Moreover, multiple groups have shown that the risk alleles of *ANRIL* variants were significantly associated with down-regulation of *ANRIL* expression (6–13). However, inconsistent findings were also reported (14), which makes the link between *ANRIL* expression and CAD/MI controversial. Therefore, functional studies are needed to establish the link between *ANRIL* expression and CAD/MI.

lncRNAs have various regulatory roles such as chromosome dosage-compensation, genetic imprinting, epigenetic regulation, cell cycle control, transcription, translation, splicing, and cell differentiation mediated by RNA–RNA, RNA–DNA, or RNA–protein interactions (8–10, 14). Several studies suggested *cis*- and *trans*-gene regulatory functions of *ANRIL* through epigenetic mechanisms (9, 10, 14). Recent studies have implicated lncRNAs in the regulation of many biological processes and other diseases such as cancer; however, the molecular mechanism by which lncRNAs regulate the pathogenesis of CAD is not well-studied (9, 14). Because *ANRIL* belongs to a family of lncRNAs, we hypothesized that it plays a crucial role in the development of atherosclerosis, CAD, and MI by regulating expression and function of other downstream target genes.

In this study, we first studied the regulatory role of *ANRIL* in endothelial cell functions, including monocyte adhesion to ECs, TEM, and EC migration, which are the cellular processes directly relevant to atherosclerosis and CAD. Our data strongly link the function of *ANRIL* to EC functions related to atherosclerosis and CAD. This enabled us to further study a specific molecular mechanism by which *ANRIL* regulates functions of endothelial cells through identifying and characterizing its downstream target genes. We found that *ANRIL* regulates the expression levels of multiple downstream genes in endothelial cells. Moreover, we identified three *ANRIL* downstream genes, *CLIP1*, *EZR*, and *LYVE1*, which were involved in rescuing functional defects of KD of *ANRIL* expression by *ANRIL* siRNA (si*ANRIL*). These data functionally validate *ANRIL* in ECs with an essential role in CAD and identify a new molecular mechanism by which *ANRIL* may regulate the pathogenesis of atherosclerosis and CAD.

Results

ANRIL transcript DQ485454 is more abundantly expressed than the full-length transcript in endothelial cells

Three *ANRIL* transcripts were annotated as *NR_003529* (the 3,857-bp full-length *ANRIL* transcript), *DQ485454* (2,659-bp transcript), and EU741058 (short 688-bp transcript) (NCBI database). Our analysis of Fig. 2 in a study reported by Holdt *et al.* (10) showed that in atherosclerotic plaques, the expression level of the *DQ485454* transcript was >6-fold higher (>750 copies/10^7 copies of *BA* as a housekeeping gene) than the levels of full-length *NR_003529* transcript (100–120 copies) or *EU741058* transcript (85–90 copies). Therefore, our studies here focused on the *DQ485454* transcript.

To study the expression profile of *ANRIL* (*DQ485454*) in cells and tissues relevant to CAD, we characterized multiple cell types for the endogenous expression level of *ANRIL* using real-time RT-PCR analysis. Three different types of human ECs (human coronary artery EC (HCAEC), human umbilical vascular EC (HUVEC), and an EC cell line EA.hy926) showed a comparable expression level of *ANRIL* (Fig. 1*A*). THP-1 monocytes expressed much less *ANRIL* than ECs (Fig. 1*A*). As in atherosclerotic plaques reported by Holdt *et al.* (10), we showed that the expression level of the *DQ485454* transcript was at least 7-fold higher in three types of human ECs than the full-length transcript *NR_003529* (Fig. 1*B*).

To determine the subcellular localization of *ANRIL* RNA (*DQ485454*), we isolated nuclear and cytoplasmic RNA samples from ECs and performed real-time RT-PCR analysis. Control *U6* RNA was mostly localized in the nucleus, whereas Lys-tRNA was mostly localized in the cytoplasm (Fig. 1*C*). Similar to U6 RNA and different from Lys-tRNA, *ANRIL* RNA was detected in both the nucleus and cytoplasm, but its expression level was about 4-fold higher in the nucleus than in the cytoplasm (Fig. 1*C*). The data suggest that *ANRIL* is more likely to demonstrate functions of the nuclear RNAs.

Down-regulation of ANRIL transcript DQ485454 in CAD coronary arteries

Total RNA samples were isolated from coronary arteries from five CAD patients and five age-matched non-CAD study subjects and used for real-time RT-PCR analysis. The expression level of *ANRIL* transcript *DQ485454* was significantly lower in the CAD group than in the non-CAD control group (Fig. 1*D*). We also analyzed the expression levels of neighboring genes. The expression level of *CDNK2B*, but not *CDKN2A* or *MTAP*, was significantly lower in the CAD group than in the non-CAD control group (Fig. 1*D*).

As inflammation is a key factor in the development of CAD, we examined whether *ANRIL DQ485454* affects the expression level of *IL1B* encoding IL-1β and *CCL2* encoding MCP-1, two factors critically involved in atherosclerotic CAD (16, 17). Transfection of human coronary artery ECs (HCAECs) with an

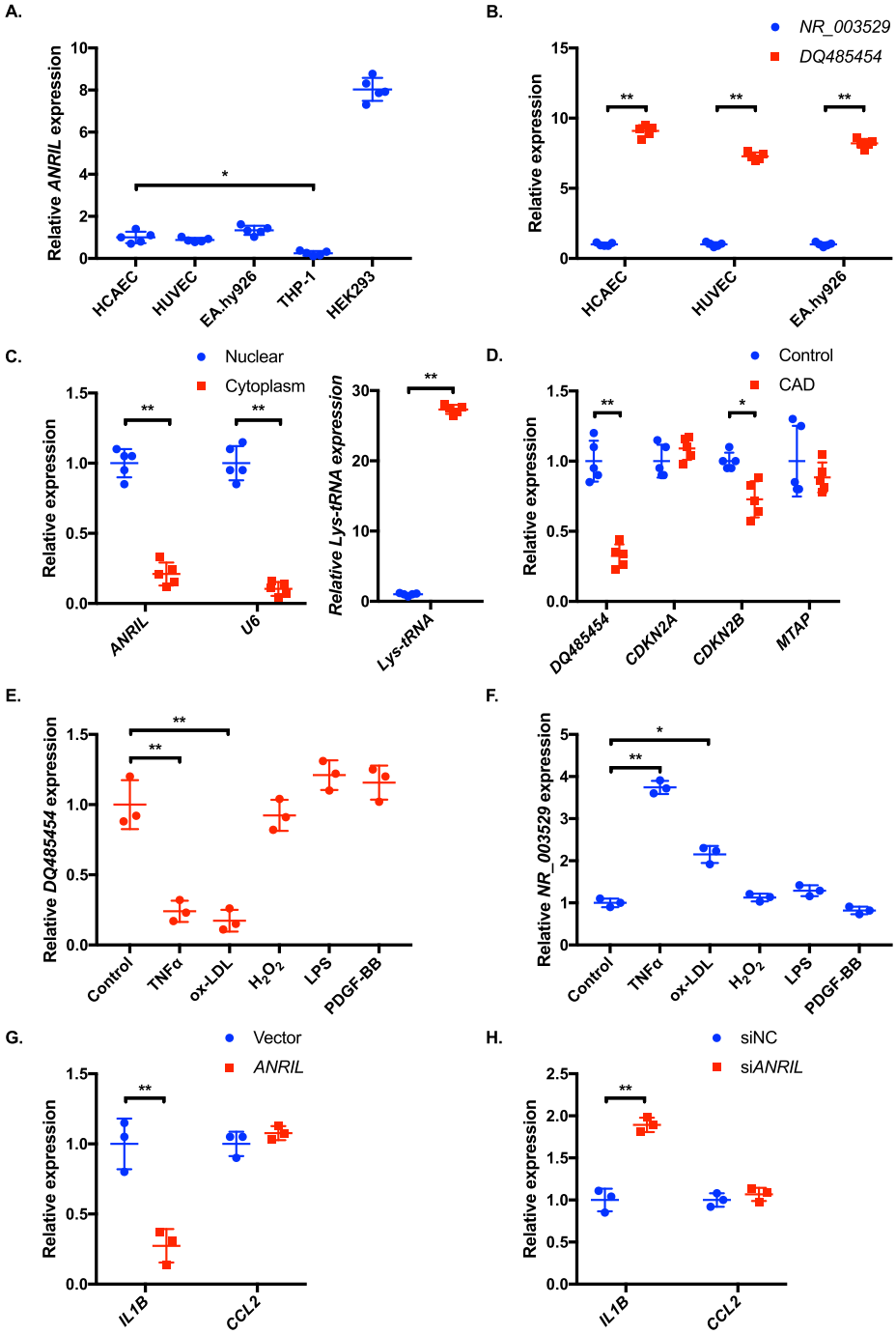

Figure 1. The *ANRIL* transcript *DQ485454* is the major isoform in endothelial cells and down-regulated in CAD coronary arteries. *A*, relative expression levels of *ANRIL* were determined by qRT-PCR from different cells. *B*, relative expression levels of the two major transcripts of *ANRIL*, *DQ485454*, and *NR_003529* (full-length) were determined by qRT-PCR from different endothelial cells. *C*, relative expression levels of *ANRIL* transcript *DQ485454* in the nucleus and cytoplasm of HCAECs. *U6* RNA and Lys-tRNA were used as positive and negative controls, respectively. *D*, relative expression levels of *DQ485454* and its neighboring genes in coronary artery tissue samples from CAD patients and non-CAD individuals. *E*, effect of inflammatory cytokines, TNFα (20 ng/ml), ox-LDL (50 μg/ml), H_2O_2 (200 μM), LPS (1 μg/ml), and PDGF-BB (10 ng/ml), on expression of *DQ485454* in HCAECs ($n = 3$). *F*, effect of inflammatory cytokines, TNFα (20 ng/ml), ox-LDL (50 μg/ml), H_2O_2 (200 μM), LPS (1 μg/ml), and PDGF-BB (10 ng/ml), on expression of *NR_003529* in HCAECs ($n = 3$). *G*, effect of *ANRIL* overexpression (*DQ485454*) on inflammatory markers in HCAECs, *IL1B* (encoding IL-1β), and *CCL2* (encoding MCP-1). *H*, effect of knockdown of *ANRIL* transcript *DQ485454* on inflammatory markers in HCAECs. *, $p < 0.05$; **, $p < 0.01$. Only statistically significant differences are marked with *asterisks*. *Error bars*, S.D.

overexpression plasmid for *ANRIL DQ485454* significantly reduced the expression level of *IL1B*, but not *CCL2*, compared with the empty vector control (Fig. 1*E*). Knockdown of *ANRIL DQ485454* using si*ANRIL* significantly increased the expression level of *IL1B*, but not *CCL2* (Fig. 1*F*). On the other hand, expression of *ANRIL* is sensitive to inflammatory responses. As shown in Fig. 1*G*, TNFα and ox-LDL cholesterol, but not H_2O_2, significantly reduced the expression level of *ANRIL* transcript *DQ485454* but increased the expression level of the full-length ANRIL (*NR_003529*) (Fig. 1*H*).

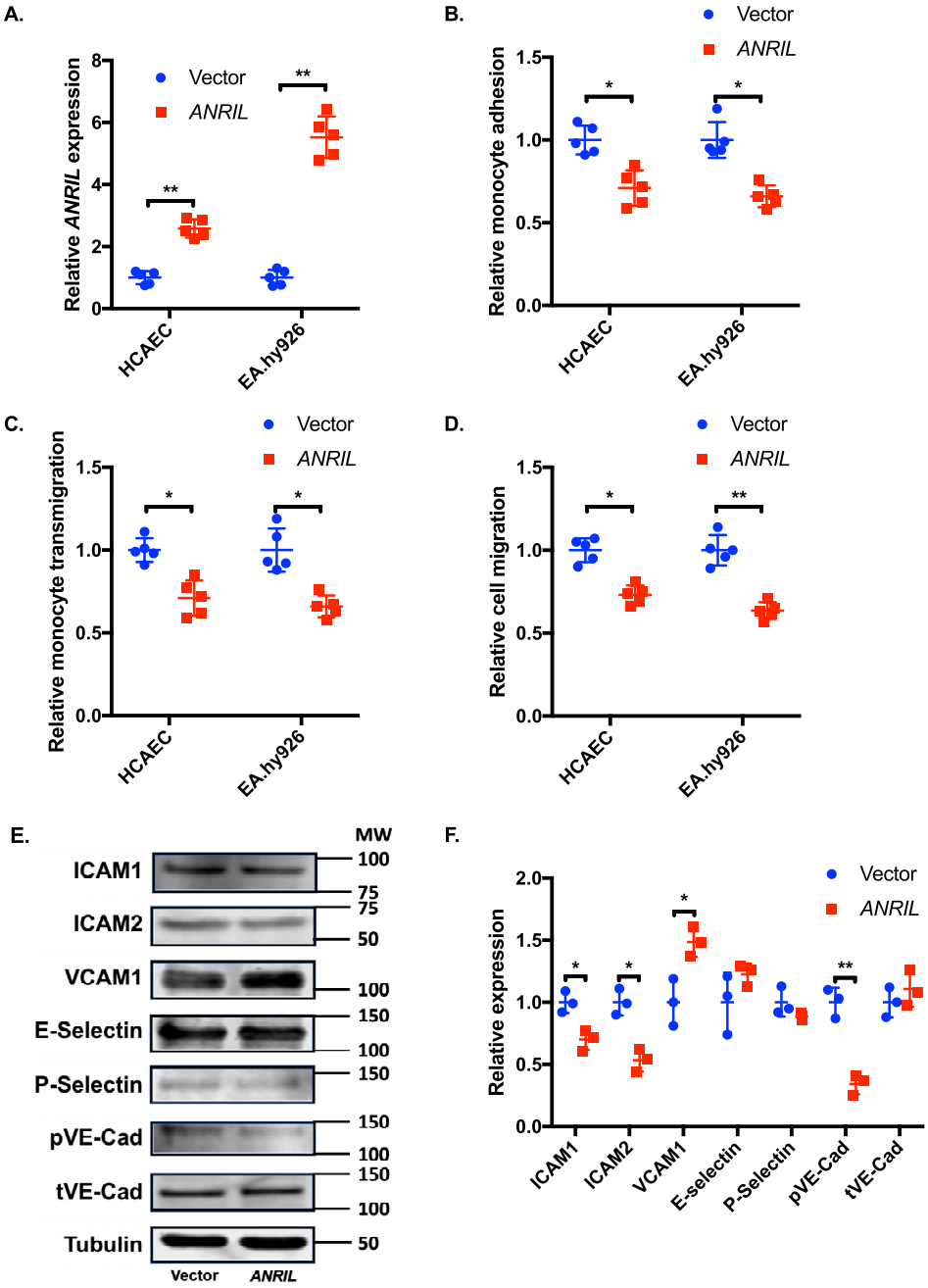

Figure 2. Effects of overexpression of *ANRIL* (*DQ485454*) on EC functions and expression of cell adhesion molecules. *A*, relative expression of *ANRIL* (*DQ485454*) in HCAEC and EA.hy926 cells by transient transfection with plasmids, pcDNA3.1 or pcDNA3.1-*ANRIL*. *B*, monocyte adhesion to HCAEC and EA.hy926 cells transfected with plasmids, pcDNA3.1 or pcDNA3.1-*ANRIL* ($n = 5$). *C*, TEM with HCAEC and EA.hy926 cells transfected with plasmids, pcDNA3.1 or pcDNA3.1-*ANRIL* ($n = 5$). *D*, migration of HCAEC and EA.hy926 cells transfected with plasmids, pcDNA3.1 or pcDNA3.1-*ANRIL* ($n = 5$). *E*, Western blot analysis of cell adhesion proteins (ICAM-1, ICAM-2, VCAM-1, E-selectin, P-selectin, pVE-Cad, and tVE-Cad) using HCAECs transfected with plasmids, pcDNA3.1 or pcDNA3.1-*ANRIL* ($n = 3$). Tubulin was used as a loading control. *F*, Western blotting images in *E* were quantified and plotted. Data were normalized to the baseline Tubulin expression, which was defined as 1.0. *, $p < 0.05$; **, $p < 0.01$. Only statistically significant differences are marked with *asterisks*. *Error bars*, S.D.

Overexpression of ANRIL (DQ485454) in endothelial cells significantly reduces monocyte adhesion to ECs, TEM, and EC migration

Based on the finding of down-regulation of *ANRIL* (*DQ485454*) in CAD coronary arteries, we hypothesized that *ANRIL* (*DQ485454*) is involved in the development of CAD. To elucidate the role of *ANRIL* in CAD, we characterized EC functions directly involved in the pathogenesis of CAD, including monocyte adhesion to ECs, TEM, and EC migration. We successfully overexpressed *ANRIL* in HCAECs and EA.hy926 ECs by transient transfection of an expression plasmid for *ANRIL* (*DQ485454*) (empty vector as control) as shown by real-time RT-PCR analysis (Fig. 2*A*). Overexpression of the *DQ485454* transcript did not affect the expression level of other major transcripts of *ANRIL* (Fig. S1*A*). Overexpression of *ANRIL* (*DQ485454*) significantly inhibited adhesion of THP-1 cells to HCAECs and EA.hy926 cells (Fig. 2*B*). Similarly, overexpression of *ANRIL* (*DQ485454*) significantly inhibited transmigra-

tion of THP-1 cells across a layer of HCAECs and EA.hy926 cells (Fig. 2*C*). Moreover, overexpression of *ANRIL* (*DQ485454*) significantly inhibited migration of HCAECs and EA.hy926 cells (Fig. 2*D*). These data suggest that overexpression of *ANRIL* (*DQ485454*) blocks monocyte adhesion to ECs, TEM, and EC migration, the initiation processes for the development of atherosclerotic CAD.

Monocyte adhesion to ECs and TEM are associated with increased expression levels of some cell adhesion molecules, including ICAM1, ICAM2, VCAM1, E-selectin, P-selectin, and VE-cadherin (1, 2, 12, 18, 19). Therefore, we analyzed the effects of overexpression of *ANRIL* (*DQ485454*) on expression levels of endothelial cell adhesion molecules. Western blot analysis with total cellular extracts showed that overexpression of *ANRIL* (*DQ485454*) significantly reduced the expression levels of ICAM1, ICAM2, and phosphorylated VE-cadherin in ECs (Fig. 2, *E* and *F*). In contrast, overexpression of *ANRIL* significantly increased the expression level of VCAM1 but did not have a significant effect on E-selectin, P-selectin, and total VE-cadherin (Fig. 2, *E* and *F*). Similar results were obtained with membrane protein extracts isolated using biotinylation (Fig. S1*C*).

Knockdown (KD) of the expression level of ANRIL in endothelial cells significantly increases monocyte adhesion to ECs, TEM, and EC migration

To further elucidate the role of *ANRIL* in EC functions directly involved in the pathogenesis of CAD, we knocked down the expression of *ANRIL* (*DQ485454*) in ECs by transient transfection of an *ANRIL*-specific siRNA (scrambled siRNA as control). Real-time RT-PCR analysis showed that the expression level of *ANRIL* (*DQ485454*) was successfully knocked down by 75–85% (Fig. 3*A*). Knockdown of the *DQ484454 ANRIL* transcript did not affect the expression level of other major transcripts of *ANRIL* (Fig. S1*D*). Knockdown of *ANRIL* expression in endothelial cells significantly increased adhesion of THP-1 cells to HCAECs and EA.hy926 cells (Fig. 3*B*) and transmigration of THP-1 cells across HCAECs and EA.hy926 cells (Fig. 3*C*). For EC migration, *ANRIL* knockdown significantly increased migration of HCAECs and EA.hy926 cells (Fig. 3*D*).

Knockdown of *ANRIL* expression in endothelial cells significantly increased the expression levels of endothelial cell adhesion molecules ICAM1, ICAM2, P-selectin, and phosphorylated VE-cadherin (Fig. 3, *E* and *F*). No effect was observed for *ANRIL* knockdown on the expression levels of E-selectin, VCAM1, and total VE-cadherin (Fig. 3, *E* and *F*). Similar results were obtained with membrane protein extracts isolated using biotinylation (Fig. S1*F*).

Identification of multiple downstream genes of ANRIL

Multiple, but not all, studies showed positive correlation between down-regulation of *ANRIL* and its neighboring gene *CDKN2B* (9–11, 14). We analyzed the effect of *ANRIL* on its neighboring genes in HCAECs. Overexpression of *ANRIL* significantly increased the expression level of *CDKN2B* but not two other neighboring genes, *CDKN2A* and *MTAP* (Fig. 1*B*). Knockdown of *ANRIL* significantly decreased the expression level of *CDKN2A* and *CDKN2B* but not *MTAP* (Fig. 1*E*).

To identify other novel downstream target genes of *ANRIL*, we performed global gene expression analysis using Affymetrix GeneChip arrays using HUVECs transfected with *ANRIL*-specific siRNA or control scrambled siRNA. After adjusting for multiple testing using Benjamini and Hochberg's FDR method, we identified a list of 147 probes, which represent 110 unique genes with differential expression between the two different treatments ($q < 0.05$) (Table S1). A heat map plot was generated using 24 top-ranked genes or probes (Fig. 4*A*). Global expression profiling analysis of the six RNA samples indicated that the overall gene expression levels were similar among the six samples (Fig. S3). The top dendrogram showed that the six RNA samples were clustered into two distinct groups that matched with their treatment status (Fig. S4).

We performed enrichment analysis of biological pathways with the 110 unique genes mapped by 147 significant probes with $q < 0.05$ using ClueGO version 2.3.3 (20) to identify highly enriched pathways or biological processes from several public databases, including gene ontology (GO), KEGG, and REACTOME. Significant pathways were assigned to several functional groups based on a κ similarity score of >0.60. Interestingly, *ANRIL* regulates the EC differentiation pathway and leukocyte migration pathway, which is consistent with our experimental findings on the role of *ANRIL* in monocyte adhesion to ECs, TEM, and EC migration. The other potential pathways regulated by *ANRIL* included the negative regulation of ERK1/2 cascade, actin filament, regulation of histone methylation, and cellular response pathways (Fig. 4*B*).

We selected the top 16 genes for further validation, and 14 genes were successfully replicated with independent samples by independent semi-quantitative RT-PCR experiments (Fig. 5*A*). We were not able to detect the expression of two genes, *ABCG1* and *KIT*, due to technical problems. Moreover, we used real-time RT-PCR analysis to validate further the top 16 genes showing differential expression with KD of *ANRIL*. Our real-time RT-PCR analysis identified eight genes that showed significantly reduced expression in endothelial cells with knockdown of *ANRIL* expression (*AHNAK2*, *CLIP1*, *CXCL11*, *ENC1*, *EZR*, *LYVE1*, *WASL*, and *TNFSF10*) (Fig. 5*B*). The analysis also identified two genes (*TMEM100* and *TMEM106B*) that showed significantly increased expression in endothelial cells with KD of *ANRIL* expression (Fig. 5*B*).

Overexpression of CLIP1, EZR, and LYVE1 reverses the functional effects of knockdown of ANRIL expression

To determine whether an *ANRIL* downstream target gene is involved in EC functions regulated by *ANRIL*, we co-transfected si*ANRIL* with a target gene expression plasmid and determined whether overexpression of a target gene can reverse functional effects of si*ANRIL*. We created and analyzed overexpression plasmids for the eight downstream genes down-regulated by si*ANRIL*, including *AHNAK2*, *CLIP1*, *CXCL11*, *ENC1*, *EZR*, *LYVE1*, *WASL*, and *TNFSF10*. To ensure consistency of our results in experiments using plasmids of many different candidate genes, further experiments with the overexpression plasmids of downstream genes of *ANRIL* were performed simultaneously, sharing the same pcDNA3.1 vector + siNC and pcDNA3.1 vector + si*ANRIL* cotransfected controls among the experiments with

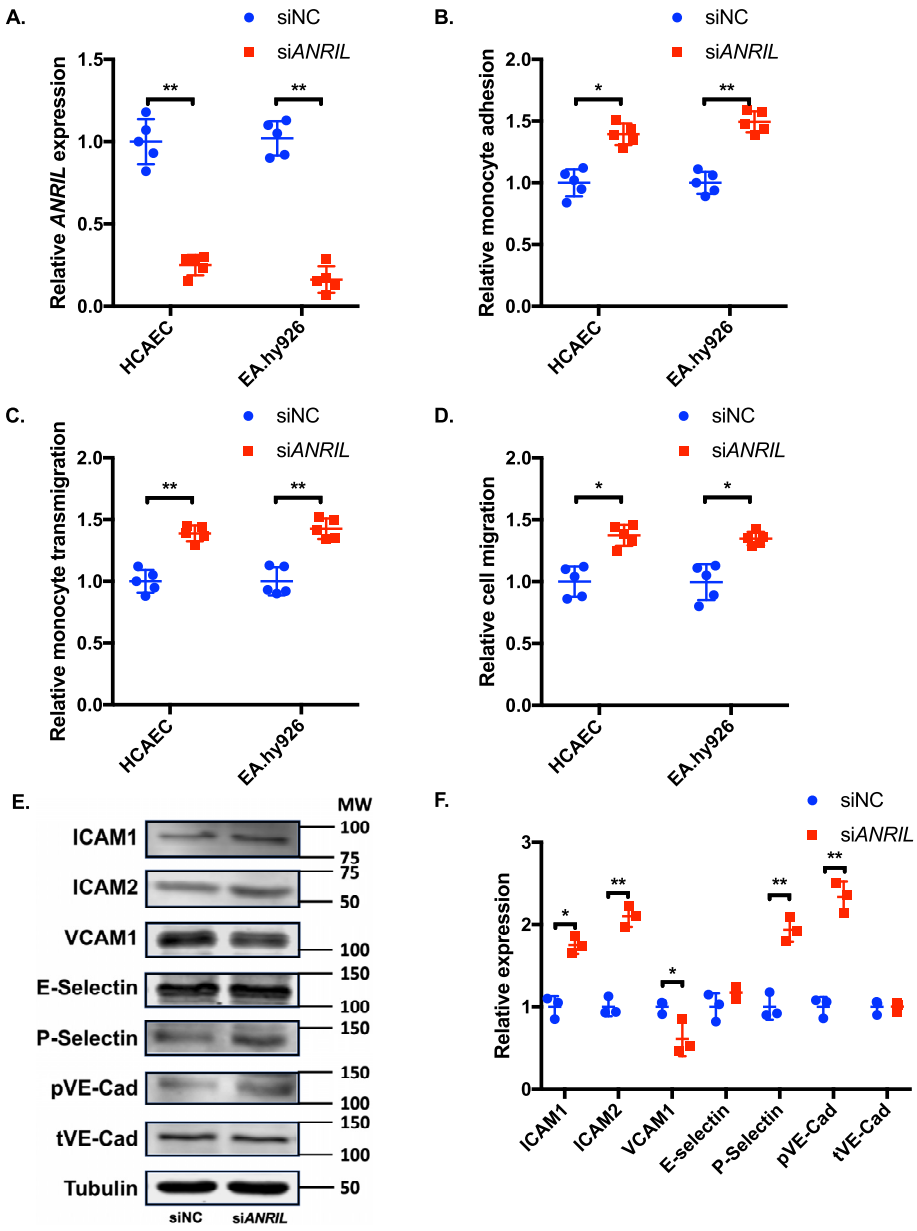

Figure 3. Effects of knockdown of *ANRIL* (*DQ485454*) on EC functions and expression of cell adhesion molecules. *A*, relative expression of ANRIL in HCAECs and EA.hy926 cells transiently transfected with either siNC or si*ANRIL*. *B*, relative quantification of monocyte adhesion to HCAEC and EA.hy926 cells transfected with siNC or si*ANRIL* ($n = 5$). *C*, relative quantification of TEM with HCAEC and EA.hy926 cells transfected with siNC or si*ANRIL* ($n = 5$). *D*, migration of HCAEC and EA.hy926 cells transfected with siNC or si*ANRIL* ($n = 5$). *E*, Western blot analysis of cell adhesion proteins (ICAM-1, ICAM-2, VCAM-1, E-selectin, P-selectin, pVE-Cad, and tVE-Cad) using HCAECs transfected with siNC or si*ANRIL* ($n = 3$). Tubulin was used as a loading control. *F*, Western blotting images in *E* were quantified and plotted. Data were normalized to the baseline tubulin expression, which was defined as 1.0. *, $p < 0.05$; **, $p < 0.01$. Only statistically significant differences are marked with *asterisks*. *Error bars*, S.D.

EA.hy926 cells (Figs. 6, 8, and 10) and HCAECs (Figs. 7, 9, and 11), respectively. Knockdown of *ANRIL* expression in ECs significantly increased monocyte adhesion to ECs, TEM, and EC migration; however, the effect was fully reversed by overexpression of *CLIP1* (Fig. 6, *A–H*) or *EZR* (Fig. 8, *A–H*) and in EA.hy926 cells. Similar rescue findings were observed for *CLIP1* (Fig. 7) and *EZR* (Fig. 9) in HCAECs for monocyte adhesion to ECs and TEM. For EC migration, *CLIP1* but not *EZR* rescued the effect of knockdown of *ANRIL* (Figs. 7 and 9). Similarly, rescue was observed with overexpression of *LYVE1* for monocyte adhesion to ECs and TEM, but not for EC migration in EA.hy926 cells (Fig. 10, *A–H*). *LYVE1* rescue was observed for monocyte adhesion to ECs, TEM, and EC migration in HCAECs (Fig. 11, *A–H*). In addition, overexpression of *CLIP1*, *EZR*, or *LYVE1* decreased the expression level of VCAM1 and showed some effects on expression of some other EC adhesion molecules (ICAM2 or E-selectin by CLIP1 and ICAM1 by EZR) (Fig. S2). These data suggest that *ANRIL* regulates monocyte adhesion to ECs, TEM, and EC migration by regulating the expression of its multiple downstream genes *CLIP1*, *EZR*, and *LYVE1*.

Discussion

In this study, we provide experimental evidence to support the hypothesis that the lncRNA gene *ANRIL* is the disease-

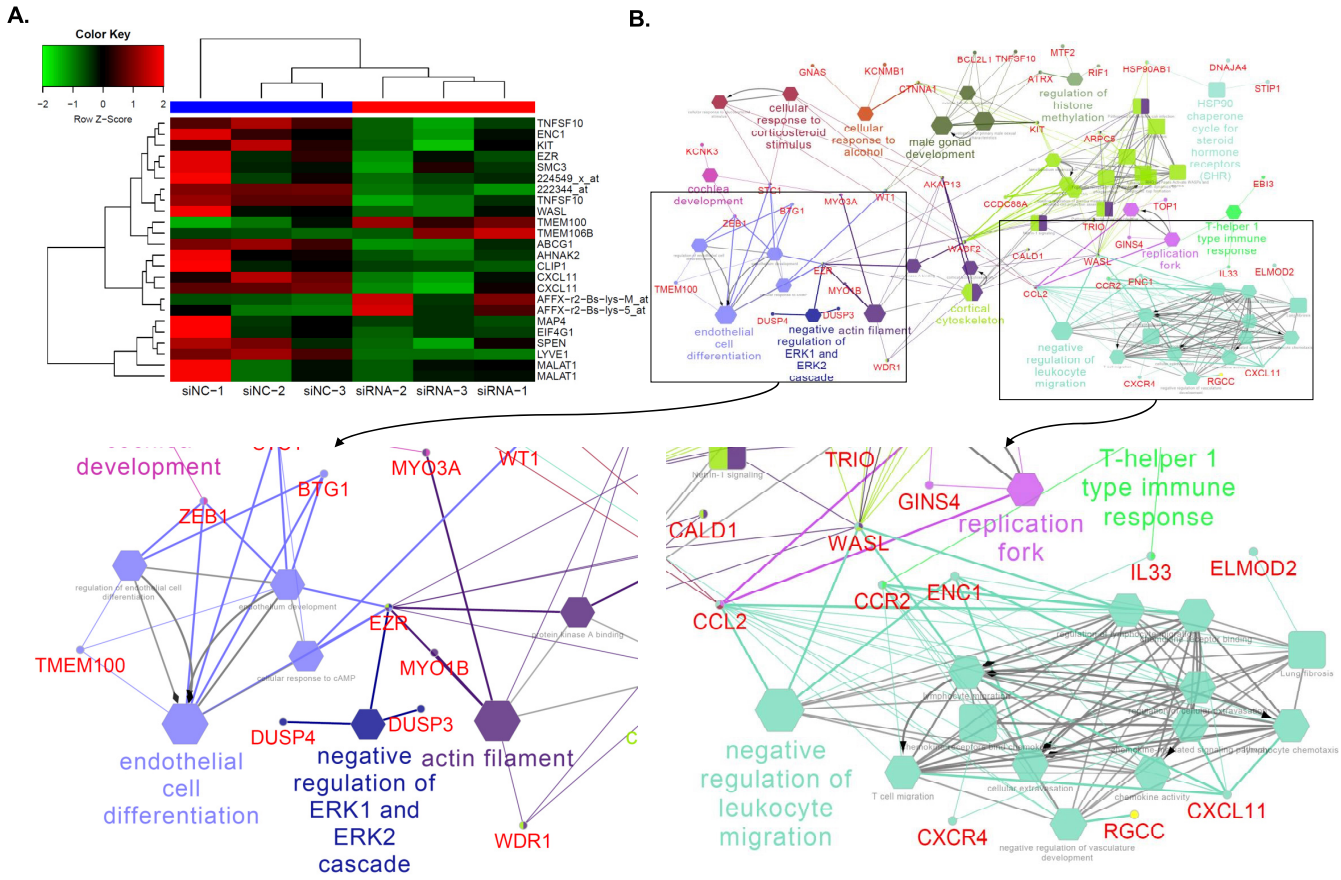

Figure 4. ANRIL downstream genes identified by global microarray analysis. *A*, heat map plot was generated using 24 top-ranked genes or probes showing differential expression levels between three siNC-transfected samples and three si*ANRIL* transfected samples. The top-ranked genes or probes were selected based on $q \leq 0.001$ after adjusting for multiple testing using the FDR method. The *top* dendrogram shows that the six RNA samples were clustered into two distinct groups that matched their treatment status. *B*, enrichment analysis of 110 unique *ANRIL* downstream genes (mapped by 147 probes with $q < 0.05$) identified 54 significant pathways. *Big* and *small nodes* represent biological pathways and their associated genes, respectively. The 54 significant biological pathways were clustered into 22 functional groups due to shared genes (κ similarity score > 0.6) as shown by *node colors*. The *node shape* indicates the sources of pathways. The *edge* reflects the known relationships in the GO database. The representative of each functional group was selected based on enrichment *p* value and GO hierarchy.

causing gene for CAD at the chromosome 9p21 genetic locus identified by GWAS. Genome-wide association is the most effective strategy to identify genomic variants and loci associated with human diseases (4, 5, 10, 14). However, most of these genomic variants identified by GWAS fall into intronic regions, noncoding regions, and gene desert areas; thus, the causal variants, causal genes, and the underlying molecular regulatory mechanisms are largely unknown (4, 5, 10, 14). Numerous studies, including our study, unequivocally associated genomic variants at the chromosome 9p21 locus with CAD in many different ethnic populations, including European, Korean, Chinese, Indian, Spanish, and Arabic ancestry populations (3–6, 8–12, 14). However, the causative gene or the driver gene for CAD at the 9p21 locus is unknown. The 9p21 locus contains several different genes, including *CDKN2A* (encoding p14 and p16), *CDKN2B* (encoding p15), *MTAP*, and *ANRIL*. It is important to define which of these genes is involved in the development of CAD (10, 11, 14). We characterized the effects of *ANRIL* overexpression and KD on EC functions directly associated with the development of CAD, including monocyte adhesion to ECs, TEM, and EC migration. Knockdown of the expression level of the major *DQ485454* transcript of *ANRIL* by siRNA significantly activated EC processes relevant to CAD, including monocyte adhesion to ECs, TEM, and EC migration (Fig. 3), suggesting that *ANRIL* KD may increase the risk of CAD. On the other hand, overexpression of the major *ANRIL* transcript *DQ485454* significantly reduced monocyte adhesion to ECs, TEM, and EC migration (Fig. 2), suggesting that overexpression of *ANRIL* may be protective of CAD risk. Holdt *et al.* (10) showed that the expression level of *ANRIL* transcript *DQ485454* in blood samples did not differ significantly with different amounts of atherosclerotic burden in carotid arteries; however, it was significantly reduced in study subjects with heterozygous and homozygous G risk haplotypes. Moreover, the expression level of *ANRIL* transcript *DQ485454* in the plaque tissue was negatively correlated with the expression level of *MTAP*, which was found to be reduced in macrophage-rich lesions (11). These data were consistent with our finding that KD of the *DQ485454* transcript of *ANRIL* significantly increased monocyte adhesion to ECs, TEM, and EC migration, all of which were associated with the development of CAD.

The molecular mechanism by which *ANRIL* KD increases the risk of CAD is unknown. Through gene expression microarray

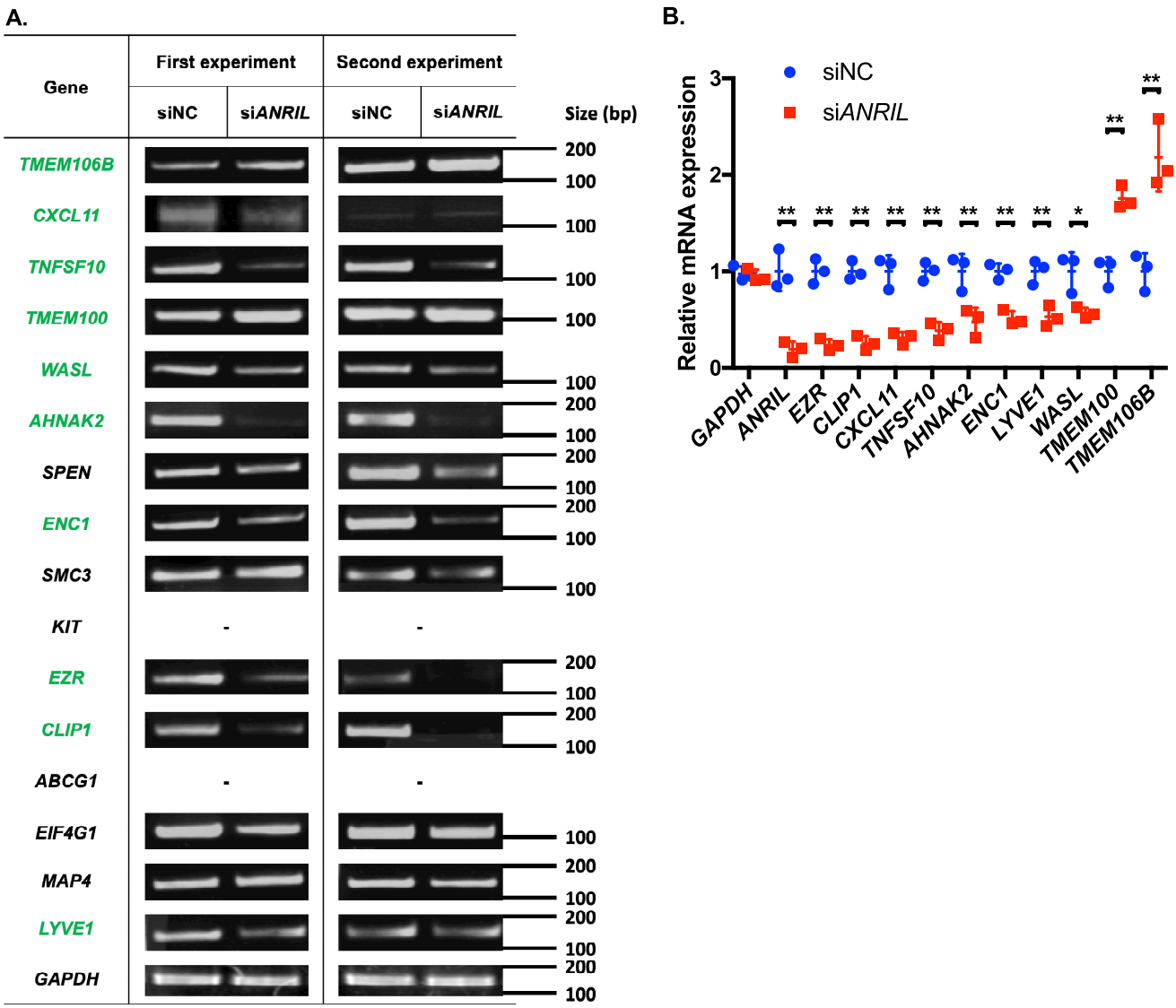

Figure 5. Validation of downstream genes of *ANRIL* from global microarray gene expression analysis using semi-quantitative RT-PCR and real-time RT-PCR analyses. *A*, semi-quantitative RT-PCR analysis using HUVECs transfected with siNC or si*ANRIL* ($n = 3$, only two shown). The top 16 protein-coding genes from the microarray analysis were selected for validation analysis. Genes were aligned by their relative -fold changes in siNC *versus* si*ANRIL*. *GAPDH* was used as an internal control. *B*, real-time qRT-PCR analysis to validate *ANRIL*-regulated genes using HUVECs transfected with siNC or si*ANRIL* ($n = 3$). Data were normalized to the baseline *GAPDH* expression, which was defined as 1.0. *, $p < 0.05$; **, $p < 0.01$. Only statistically significant differences are marked with *asterisks*. *Error bars*, S.D.

analysis, we identified and validated 10 target genes downstream of *ANRIL*. *ANRIL* KD significantly down-regulated the expression levels of *AHNAK2*, *CLIP1*, *CXCL11*, *ENC1*, *EZR*, *LYVE1*, *TNFSF10*, and *WASL* genes and up-regulated the expression levels of *TMEM100 and TMEM106B* genes (Fig. 5). Our rescue experiments with the eight downstream genes down-regulated by si*ANRIL* showed that overexpression of *CLIP1*, *EZR*, and *LYVE1* reversed the effects of KD of *ANRIL* on monocyte adhesion to ECs, TEM, and EC migration (Figs. 6–8). Our data suggest that *ANRIL* deregulation in endothelial cells regulates key EC functions by regulating the expression levels of key downstream genes *CLIP1*, *EZR*, and *LYVE1*. The molecular mechanism by which *ANRIL* regulates the expression of *CLIP1*, *EZR*, *LYVE1*, and other target genes (Fig. 5) as well as its neighboring gene *CDKN2B* (Fig. 1*D*) is unknown and will require further studies in the future.

CLIP1 encodes a cytoplasmic linker protein, CLIP-170, which was a founding member of the microtubule plus end–tracking protein (+TIP) family, and KD of *CLIP1* expression by siRNAs inhibited HUVEC migration and capillary tube formation, but not proliferation (21, 22). Similarly, KD of *EZR* expression inhibited HUVEC migration and capillary tube formation (23). Moreover, ezrin was shown to bind to L-selectin, and KD of *EZR* in monocytes impaired recruitment of monocytes to activated ECs (24). LYVE1 was shown to promote migration of lymphatic ECs induced by VEGFA (25). Moreover, LYVE1 was shown to be required for docking of tissue dendritic cells to the lymphatic vessel endothelium and transmigration of dendritic cells across ECs into the lumen (26). These findings strongly support our conclusion that *ANRIL* regulates monocyte adhesion to ECs, TEM, and EC migration by regulating the expression levels of *CLIP1*, *EZR*, and *LYVE1*.

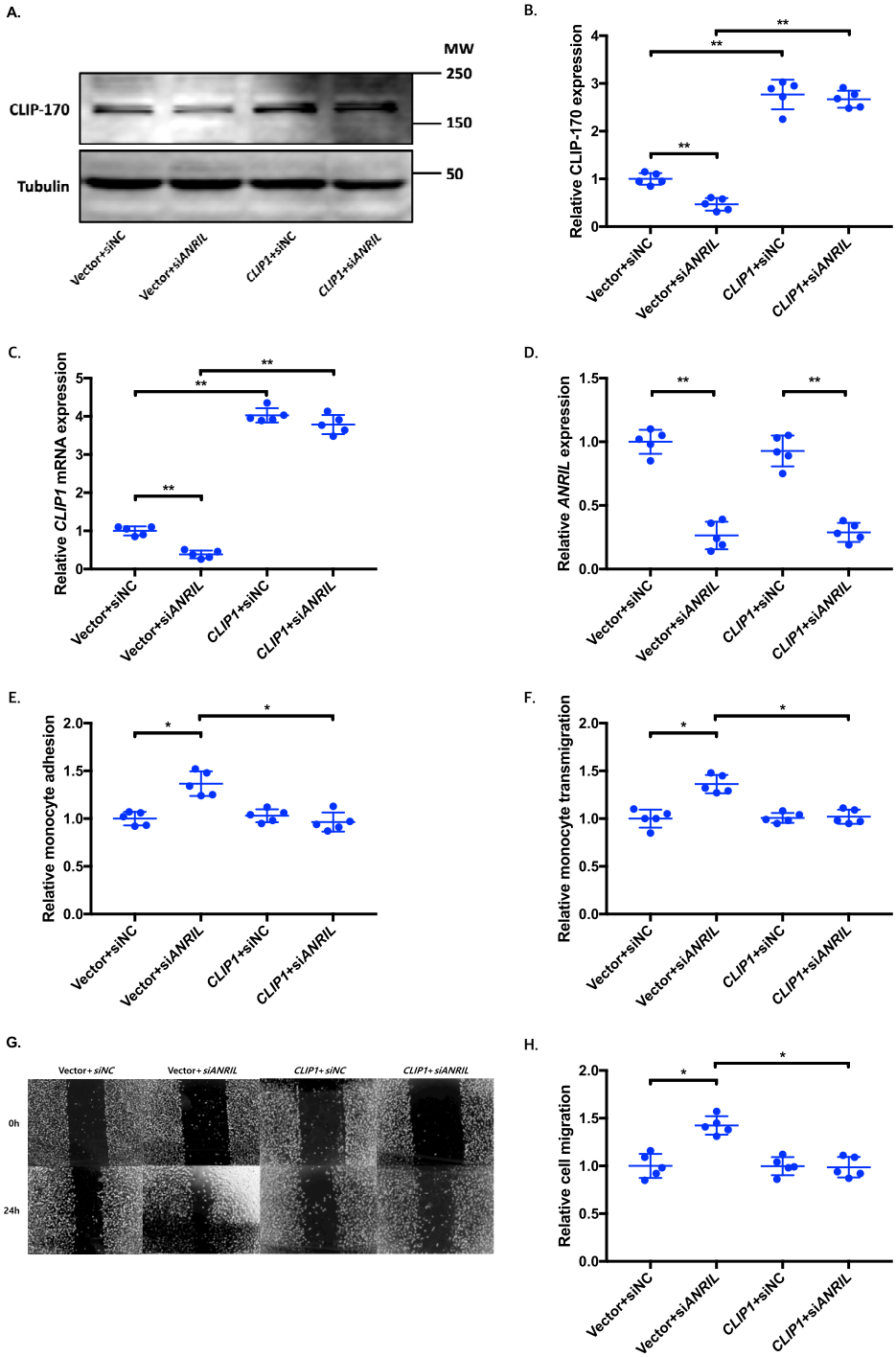

Figure 6. Overexpression of *CLIP1* reverses the functional effects of *ANRIL* knockdown in EA.hy926 cells. *A–H*, four different groups of EA.hy926 cells co-transfected with pcDNA3.1 vector + siNC, pcDNA3.1 vector + si*ANRIL*, pcDNA3.1-*CLIP1* + siNC, and pcDNA3.1-*CLIP1* + si*ANRIL*, respectively, were used for further analysis ($n = 5$). To maximize accuracy and consistency in data, experiments in EA.hy926 cells with *CLIP1* (Fig. 6), *EZR* (Fig. 8), and *LYVE1* (Fig. 10) overexpression plasmids were performed simultaneously, sharing the same pcDNA3.1 vector + siNC and pcDNA3.1 vector + si*ANRIL* cotransfected controls. Data were normalized to the value of each pcDNA3.1 vector + siNC group, which was defined as 1.0. *, $p < 0.05$; **, $p < 0.01$. Only statistically significant differences are marked with *asterisks*. *A*, protein expression of CLIP-170 was measured in the four different EA.hy926 cell groups using Western blot analysis. Tubulin was used as a loading control. *B*, Western blotting images in *A* were quantified and plotted. *C*, relative overexpression of *CLIP1* was determined in the four different EA.hy926 cell groups through qRT-PCR analysis, and the results were plotted. *D*, relative knockdown efficiency of si*ANRIL* in the four different EA.hy926 cell groups was determined through qRT-PCR analysis, and the results were plotted. *E*, adhesion of THP-1 cells to the four different EA.hy926 cell groups was quantified after 1 h of co-incubation, and the results were plotted. *F*, transmigration of THP-1 cells across a layer of the four different EA.hy926 cell groups was quantified after 24 h of co-incubation, and the results were plotted. *G*, raw images of the four different EA.hy926 cell groups at the 0- and 24-h time points during their migration. *H*, the area of the changes in the healed wound shown in *G* was quantified and plotted. *Error bars*, S.D.

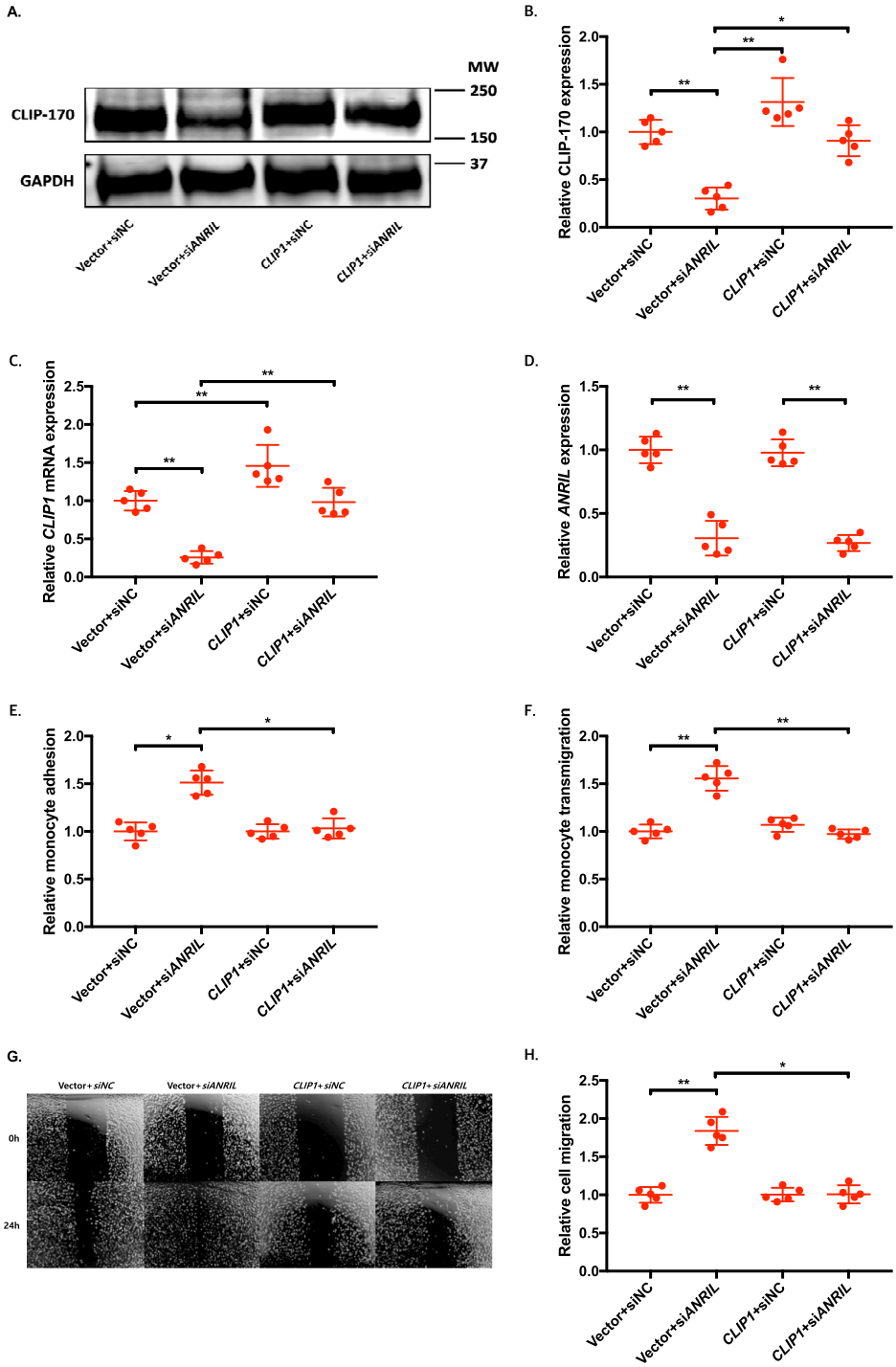

Figure 7. Overexpression of *CLIP1* reverses the functional effects of *ANRIL* knockdown in HCAECs. *A–H*, four different groups of HCAECs co-transfected with pcDNA3.1 vector + siNC, pcDNA3.1 vector + si*ANRIL*, pcDNA3.1-*CLIP1* + siNC, and pcDNA3.1-*CLIP1* + si*ANRIL*, respectively, were used for further analysis ($n = 5$). To maximize accuracy and consistency in data, experiments in HCAECs with *CLIP1* (Fig. 7), *EZR* (Fig. 9), and *LYVE1* (Fig. 11) overexpression plasmids were performed simultaneously, sharing the same pcDNA3.1 vector + siNC and pcDNA3.1 vector + si*ANRIL* cotransfected controls. Data were normalized to the value of each pcDNA3.1 vector + siNC group, which was defined as 1.0. *, $p < 0.05$; **, $p < 0.01$. Only statistically significant differences are marked with *asterisks*. *A*, protein expression of CLIP-170 was measured in the four different HCAEC groups using Western blot analysis. GAPDH was used as a loading control. *B*, Western blotting images in *A* were quantified and plotted. *C*, relative overexpression of *CLIP1* was determined in the four different HCAEC groups through qRT-PCR analysis, and the results were plotted. *D*, relative knockdown efficiency of si*ANRIL* in the four different HCAEC groups was determined through qRT-PCR analysis, and the results were plotted. *E*, adhesion of THP-1 cells to the four different HCAEC groups was quantified after 1 h of co-incubation, and the results were plotted. *F*, transmigration of THP-1 cells across a layer of the four different HCAEC groups was quantified after 24 h of co-incubation, and the results were plotted. *G*, raw images of the four different HCAEC groups at the 0- and 24-h time points during their migration. *H*, the area of the changes in the healed wound shown in *G* was quantified and plotted. *Error bars*, S.D.

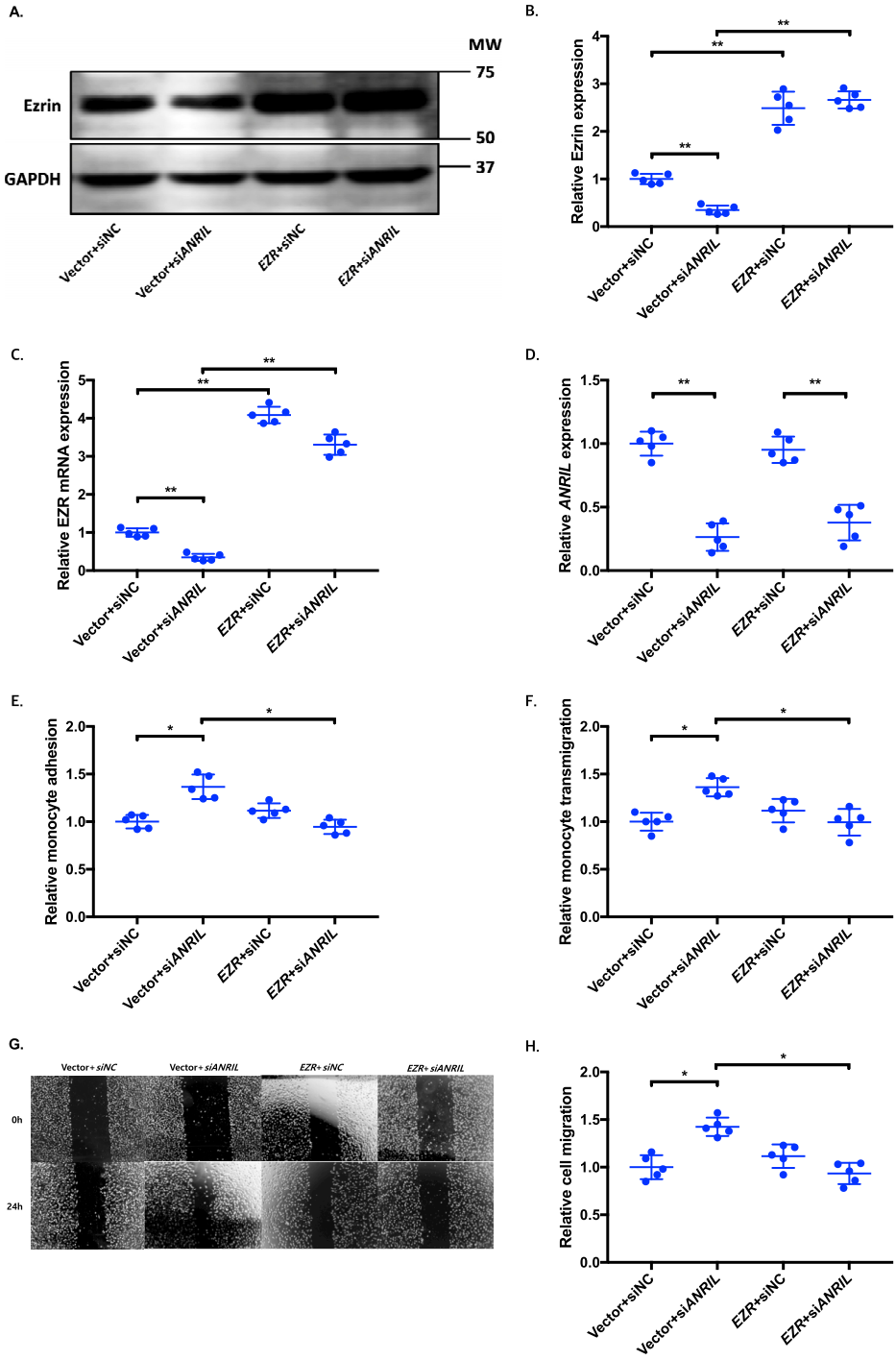

Figure 8. Overexpression of *EZR* reverses the functional effects of *ANRIL* knockdown in EA.hy926 cells. *A–H*, four different groups of EA.hy926 cells co-transfected with pcDNA3.1 vector + siNC, pcDNA3.1 vector + si*ANRIL*, pcDNA3.1-*EZR* + siNC, and pcDNA3.1-*EZR* + si*ANRIL*, respectively, were used for further analysis ($n = 5$). To maximize accuracy and consistency in data, experiments in EA.hy926 cells with *CLIP1* (Fig. 6), *EZR* (Fig. 8), and *LYVE1* (Fig. 10) overexpression plasmids were performed simultaneously, sharing the same pcDNA3.1 vector + siNC and pcDNA3.1 vector + si*ANRIL* cotransfected controls. Data were normalized to the value of each pcDNA3.1 vector + siNC group, which was defined as 1.0. *, $p < 0.05$; **, $p < 0.01$. Only statistically significant differences are marked with *asterisks*. *A*, protein expression of ezrin was measured in the four different EA.hy926 cell groups using Western blot analysis. GAPDH was used as a loading control. *B*, Western blotting images in *A* were quantified and plotted. *C*, relative overexpression of *EZR* was determined in the four different EA.hy926 cell groups through qRT-PCR analysis, and the results were plotted. *D*, relative knockdown efficiency of si*ANRIL* in the four different EA.hy926 cell groups was determined through qRT-PCR analysis, and the results were plotted. *E*, adhesion of THP-1 cells to the four different EA.hy926 cell groups was quantified after 1 h of co-incubation, and the results were plotted. *F*, transmigration of THP-1 cells across a layer of the four different EA.hy926 cell groups was quantified after 24 h of co-incubation, and the results were plotted. *G*, raw images of the four different EA.hy926 cell groups at the 0- and 24-h time points during their migration. For control groups, images of the vector + siNC and vector + si*ANRIL* cotransfected controls in Fig. 6*G* are reused. *H*, the area of the changes in the healed wound shown in *G* was quantified and plotted. *Error bars*, S.D.

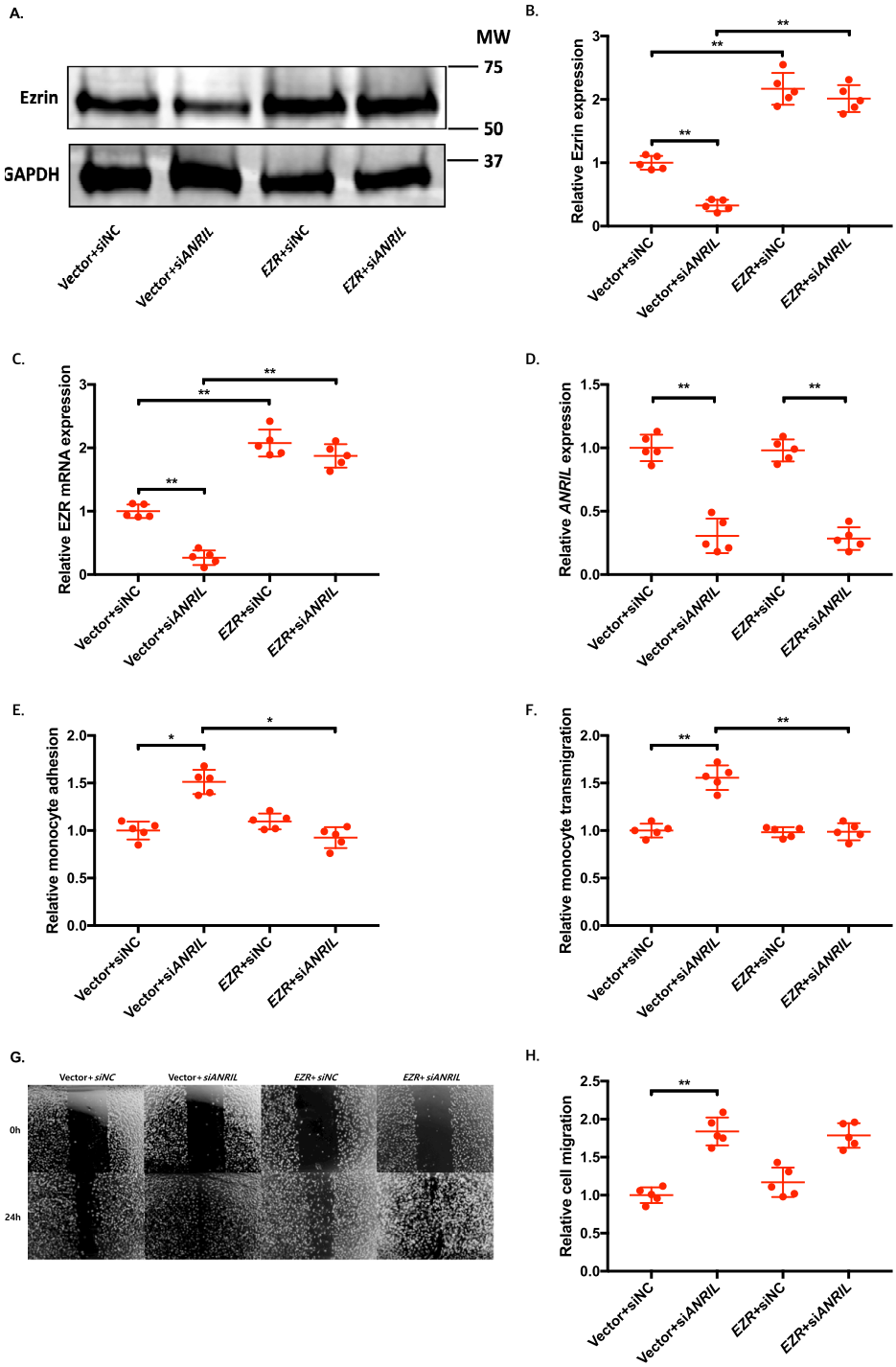

Figure 9. Overexpression of *EZR* reverses the functional effects of *ANRIL* knockdown in HCAECs. *A–H*, four different groups of HCAECs co-transfected with pcDNA3.1 vector + siNC, pcDNA3.1 vector + si*ANRIL*, pcDNA3.1-*EZR* + siNC, and pcDNA3.1-*EZR* + si*ANRIL*, respectively, were used for further analysis ($n = 5$). To maximize accuracy and consistency in data, experiments in HCAECs with *CLIP1* (Fig. 7), *EZR* (Fig. 9), and *LYVE1* (Fig. 11) overexpression plasmids were performed simultaneously, sharing the same pcDNA3.1 vector + siNC and pcDNA3.1 vector + si*ANRIL* cotransfected controls. Data were normalized to the value of each pcDNA3.1 vector + siNC group, which was defined as 1.0. *, $p < 0.05$; **, $p < 0.01$. Only statistically significant differences are marked with *asterisks*. *A*, protein expression of Ezrin was measured in the four different HCAEC groups using Western blot analysis. GAPDH was used as a loading control. *B*, Western blotting images in *A* were quantified and plotted. *C*, relative overexpression of *EZR* was determined in the four different HCAEC groups through qRT-PCR analysis, and the results were plotted. *D*, relative knockdown efficiency of si*ANRIL* in the four different HCAEC groups was determined through qRT-PCR analysis, and the results were plotted. *E*, adhesion of THP-1 cells to the four different HCAEC groups was quantified after 1 h of co-incubation, and the results were plotted. *F*, transmigration of THP-1 cells across a layer of the four different HCAEC groups was quantified after 24 h of co-incubation, and the results were plotted. *G*, raw images of the four different HCAEC groups at the 0- and 24-h time points during their migration. For control groups, images of the vector + siNC and vector + si*ANRIL* cotransfected controls in Fig. 7*G* are reused. *H*, the area of the changes in the healed wound shown in *G* was quantified and plotted. *Error bars*, S.D.

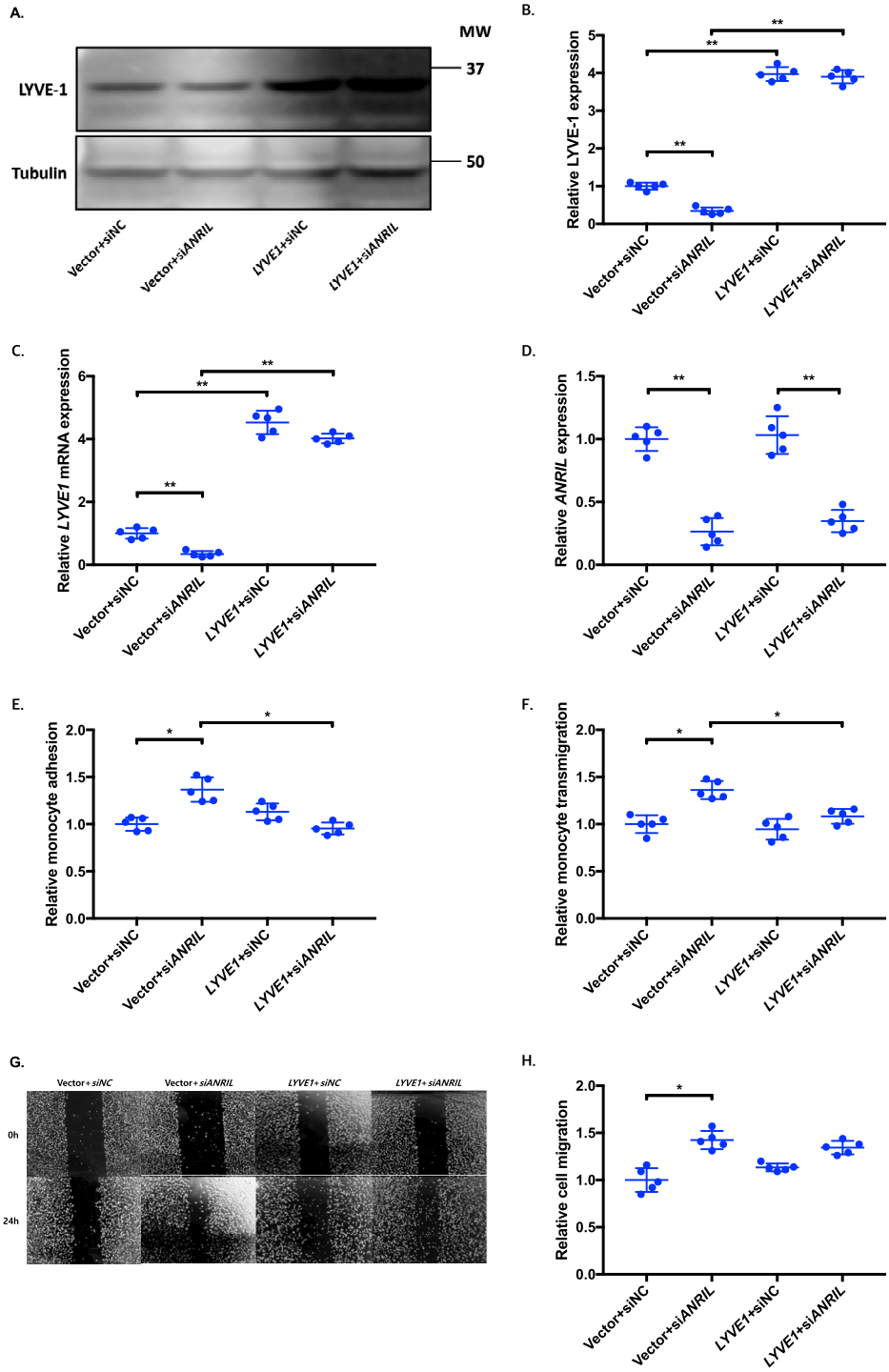

Figure 10. Overexpression of *LYVE1* reverses the functional effects of *ANRIL* knockdown in EA.hy926 cells. *A–H*, four different groups of EA.hy926 cells co-transfected with pcDNA3.1 vector + siNC, pcDNA3.1 vector + si*ANRIL*, pcDNA3.1-*LYVE1* + siNC, and pcDNA3.1-*LYVE1* + si*ANRIL*, respectively, were used for further analysis ($n = 5$). To maximize accuracy and consistency in data, experiments in EA.hy926 cells with *CLIP1* (Fig. 6), *EZR* (Fig. 8), and *LYVE1* (Fig. 10) overexpression plasmids were performed simultaneously, sharing the same pcDNA3.1 vector + siNC and pcDNA3.1 vector + si*ANRIL* cotransfected controls. Data were normalized to the value of each pcDNA3.1 vector + siNC group, which was defined as 1.0. *, $p < 0.05$; **, $p < 0.01$. Only statistically significant differences are marked with *asterisks*. *A*, protein expression of LYVE-1 was measured in the four different EA.hy926 cell groups using Western blot analysis. Tubulin was used as a loading control. *B*, Western blotting images in *A* were quantified and plotted. *C*, relative overexpression of *LYVE1* was determined in the four different EA.hy926 cell groups through qRT-PCR analysis, and the results were plotted. *D*, relative knockdown efficiency of si*ANRIL* in the four different EA.hy926 cell groups was determined through qRT-PCR analysis, and the results were plotted. *E*, adhesion of THP-1 cells to the four different EA.hy926 cell groups was quantified after 1 h of co-incubation, and the results were plotted. *F*, transmigration of THP-1 cells across a layer of the four different EA.hy926 cell groups was quantified after 24 h of co-incubation, and the results were plotted. *G*, raw images of the four different EA.hy926 cell groups at the 0- and 24-h time points during their migration. For control groups, images of the vector + siNC and vector + si*ANRIL* cotransfected controls in Fig. 6*G* are reused. *H*, the area of the changes in the healed wound shown in *G* was quantified and plotted. *Error bars*, S.D.

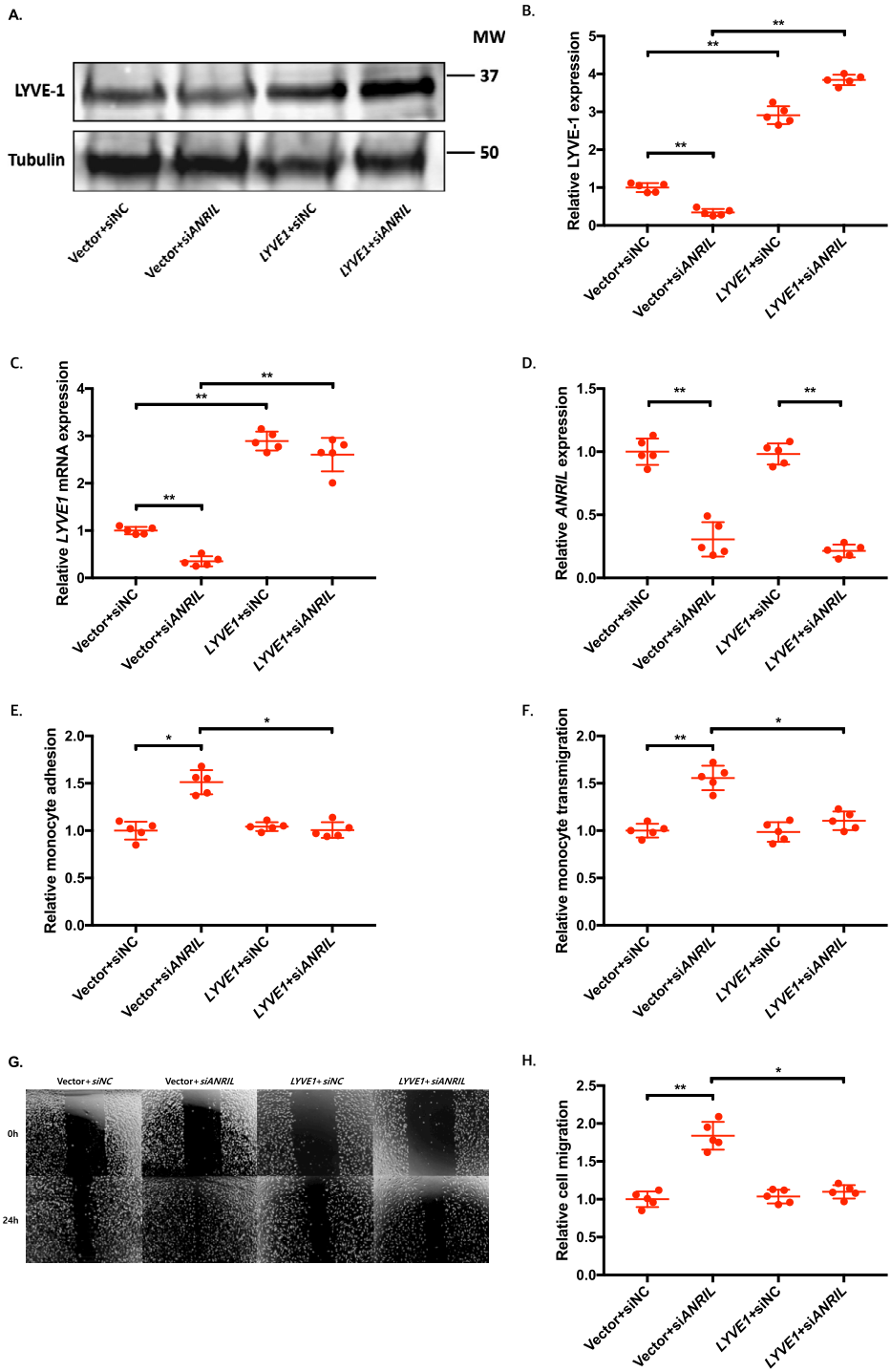

Figure 11. Overexpression of *LYVE1* reverses the functional effects of *ANRIL* knockdown in HCAECs. *A–H*, four different groups of HCAECs co-transfected with pcDNA3.1 vector + siNC, pcDNA3.1 vector + si*ANRIL*, pcDNA3.1-*LYVE1* + siNC, and pcDNA3.1-*LYVE1* + si*ANRIL*, respectively, were used for further analysis ($n = 5$). To maximize accuracy and consistency in data, experiments in HCAECs with *CLIP1* (Fig. 7), *EZR* (Fig. 9), and *LYVE1* (Fig. 11) overexpression plasmids were performed simultaneously, sharing the same pcDNA3.1 vector + siNC and pcDNA3.1 vector + si*ANRIL* cotransfected controls. Data were normalized to the value of each pcDNA3.1 vector + siNC group, which was defined as 1.0. *, $p < 0.05$; **, $p < 0.01$. Only statistically significant differences are marked with *asterisks*. *A*, protein expression of LYVE-1 was measured in the four different HCAEC groups using Western blot analysis. Tubulin was used as a loading control. *B*, Western blotting images in *A* were quantified and plotted. *C*, relative overexpression of *LYVE1* was determined in the four different HCAEC groups through qRT-PCR analysis, and the results were plotted. *D*, relative knockdown efficiency of si*ANRIL* in the four different HCAEC groups was determined through qRT-PCR analysis, and the results were plotted. *E*, adhesion of THP-1 cells to the four different HCAEC groups was quantified after 1 h of co-incubation, and the results were plotted. *F*, transmigration of THP-1 cells across a layer of the four different HCAEC groups was quantified after 24 h of co-incubation, and the results were plotted. *G*, raw images of the four different HCAEC groups at the 0- and 24-h time points during their migration. For control groups, images of the vector + siNC and vector + si*ANRIL* cotransfected controls in Fig. 7*G* are reused. *H*, the area of the changes in the healed wound shown in *G* was quantified and plotted. *Error bars*, S.D.

Macropinocytosis is an actin-driven endocytic process that is responsible for the nonselective uptake of solute molecules, nutrients, and antigens (27). Interestingly, both *CLIP1* and *EZR* are involved in macropinocytosis. CLIP-170 (encoded by *CLIP1*) was shown to be co-localized with Rab11 involved in membrane ruffle formation and macropinocytosis and phagocytosis in macrophages (22). Ezrin was shown to interact with and recruit PLEKHG6, a Rho guanine nucleotide exchange factor, both of which were required for efficient macropinocytosis (22, 28). Together with our data, we postulate that by regulating CLIP-170 and ezrin expression, *ANRIL* may mediate EC functions by regulating EC micropinocytosis, which promotes macropinocytic uptake and degradation of extracellular proteins, nutrients, and other molecules, providing the much-needed amino acids and other materials to fuel EC metabolism. Extensive future studies are needed to test this interesting possibility.

We showed that pro-inflammatory factors TNFα and ox-LDL cholesterol, but not LPS or H_2O_2, significantly down-regulated the expression of *ANRIL* transcript *DQ485454* (Fig. 1*E*) but up-regulated the long *ANRIL* transcript (*NR_003529*) (Fig. 1*F*). Our data suggest that pro-inflammatory factors differentially regulate the expression level of different *ANRIL* transcripts. A previous study showed that TNFα and IFN-γ up-regulated the expression level of a mixture of *ANRIL* transcripts, although the specific effect on *ANRIL* transcript *DQ485454* was not studied (29). It is interesting that overexpression of *ANRIL* transcript *DQ485454* significantly reduced the expression level of IL-1β, one of the most important inflammatory mediators involved in NLRP3 inflammasome activation (Fig. 1*G*), whereas an opposite effect was observed for *DQ485454* siRNA (Fig. 1*H*). Zhou *et al.* (29) showed that two si*ANRIL*s targeting exon 1 and exon 6 and affecting almost all *ANRIL* transcripts did not affect the expression levels of IL-6 and IL-8, but up-regulated their expression upon stimulation with TNFα. The specific effect on *ANRIL* transcript *DQ485454* was not studied by Zhou *et al.* (29). Together, these data suggest the existence of a possible transcript-specific effect of *ANRIL* associated with inflammatory responses, and it should be of interest to further dissect the differential effects of >20 different, alternatively spliced *ANRIL* transcripts in the future.

In summary, we have provided evidence to suggest that the *ANRIL* gene encoding an lncRNA is involved in EC functions relevant to the development of CAD. We showed that the expression level of *ANRIL* (*DQ485454*) was significantly down-regulated in CAD coronary arteries compared with non-CAD control tissue samples. We also identified 10 downstream target genes whose expression is regulated by *ANRIL* and demonstrated that *ANRIL* (*DQ485454*) regulates EC functions directly related to the development of CAD, including monocyte adhesion to ECs, TEM, and EC migration, by regulating *CLIP1*, *EZR*, and *LYVE1* expression. These findings provide valuable insights into the pathogenesis of CAD by extending our understanding of the roles and molecular mechanisms of lncRNAs in the development of CAD.

Experimental procedures

Human subjects

This study involved five CAD patients and five age-matched non-CAD study subjects (48, 53, 53, 47, 50 years of age, respectively). Total RNA was isolated from frozen coronary arteries from study subjects using TRIzol reagent (Thermo Fisher Scientific) according to the manufacturer's instructions and used for real-time RT-PCR analysis as described below. This study was approved by the Cleveland Clinic Institutional Review Board on Human Subject Research, and written consent was obtained from the subjects. This study abides by the Declaration of Helsinki principles.

Plasmids

A mammalian expression plasmid for *ANRIL* transcript *DQ485454*, referred to as pcDNA3.1-*ANRIL* (*DQ485454*), was generated by double-digestion of pcDNA3.1-*ANRIL* (*NR_003529*) with NsiI and HindIII and an addition of exon 13 through *in vitro* transcription. The pcDNA3.1-*ANRIL* (*NR_003529*) plasmid was originally created by cloning the full-length *ANRIL* transcript into XhoI and HindIII restriction sites of the pcDNA3.1 vector as described previously by us (13). The expression plasmid was verified with Sanger sequence analysis by the Genomics Core of the Cleveland Clinic Lerner Research Institute.

Mammalian expression plasmids for *ANRIL* downstream genes were created in pcDNA3.1. The Mammalian Gene Collection fully sequenced human cDNA clones of *CLIP1*, *CXCL11*, *ENC1*, *EZR*, *LYVE1*, *TMEM106B*, *TNFSF10*, and *WASL* were purchased from GE Dharmacon and subcloned into pcDNA3.1. All plasmids were individually verified by Sanger sequence analysis.

Cell culture and transfection

HCAECs (ATCC) and HUVECs (Lonza) were cultured in a phenol red–free endothelial growth medium (ATCC) supplemented with 2% fetal bovine serum (FBS), 0.4% human fibroblast growth factor, 0.1% human epidermal growth factor, 0.1% vascular endothelial growth factor, 0.1% insulin-like growth factor, 0.1% ascorbic acid, 0.1% heparin, 0.1% gentamicin/amphotericin-B, and 0.04% hydrocortisone (all from ATCC). EA.hy926, a human umbilical vascular endothelial cell line (ATCC), was cultured in Dulbecco's modified Eagle's medium with 10% FBS. Human THP-1 monocytes were obtained from ATCC and cultured in RPMI 1640 supplemented with 10% FBS. All cultures were maintained at 37 °C in a humidified atmosphere with 5% CO_2.

Transient transfection of mammalian expression plasmids and siRNAs (si*ANRIL* and negative control siRNA, or *siNC*, Integrated DNA Technologies, Skokie, IL) was performed using the nonliposomal TransIT-X2 Dynamic Delivery System (Mirus Bio, Madison, WI) according to the manufacturer's instructions.

Monocyte adhesion assays

Monocyte adhesion assays were performed as described previously (30–33). HCAECs or EA.hy926 cells were seeded into 0.2% gelatin-coated 6-well plates at a density of 500,000 cells/

well. At 70% confluence, cells were made quiescent for 24 h in the medium with 0.2% FBS and then exposed to inflammatory stress induced by 10 ng/ml TNFα (Millipore Sigma) for 12 h. After TNFα stimulation, 500,000 Calcein-AM–stained THP-1 cells were added to each well and co-incubated for 1 h. In pilot studies with EA.hy926 cells, knockdown of *ANRIL* by siRNA significantly increased the adhesion of THP-1 cells to EA.hy926 cells at time points of 1, 1.5, and 2 h, but not at 0.5 h. Therefore, we selected the time point of 1 h for later studies. Nonadhering THP-1 cells were rinsed away by washing three times with 1× Dulbecco's PBS. FITC fluorescence was measured at excitation of 488 nm and emission of 520 nm using a BioTek Synergy 2 plate reader (BioTek) to quantify the remaining attached monocytes. Five independent experiments were performed.

Assays for TEM

TEM was performed as described previously (30–33). HCAECs and EA.hy926 cells were seeded at 30,000 cells/well onto Corning Transwell filters (3-μm pore, 6.5-mm diameter) (Corning) previously coated with 0.2% gelatin and grown to confluence. Cells were made quiescent for 24 h in the medium with 0.2% FBS and exposed to 10 ng/ml TNFα for 12 h. Then, 30,000 THP-1 cells were loaded above the endothelial cells. Endothelial cells and monocytes were co-incubated for 24 h at 37 °C and 5% CO_2. In pilot studies with EA.hy926 cells, knockdown of *ANRIL* by siRNA significantly increased TEM at time points of 12, 24, 36, and 48 h. Therefore, we selected the time point of 24 h for later studies. THP-1 cells that transmigrated to the lower chamber were harvested and counted using a Beckman cell counter (Beckman Coulter). Five independent experiments were performed.

Endothelial cell migration assays

Endothelial cell migration assays were performed as described previously (31–33). HCAECs and EA.hy926 cells (500,000 cells/well) were treated with 10 ng/ml TNFα for 12 h and scratched in the middle of each well using a pipette tip. Cells were cultured inside a 37 °C and 5% CO_2 incubator for 24 h in the medium with 0.2% FBS. EC migration was evaluated by calculating the invaded area by the migratory endothelial cells under a microscope. In pilot studies with EA.hy926 cells, knockdown of *ANRIL* by siRNA significantly increased EC migration at time points of 12, 24, 36, and 48 h. Therefore, we selected the time point of 24 h for later studies. Five independent experiments were performed.

Gene expression microarray analysis

Microarray analysis was performed as previously described by us (12, 13, 32). Three sets of HUVECs were transfected with si*NC or* si*ANRIL*. Total RNA samples were isolated from the transfected cells using TRIzol reagent (Thermo Fisher Scientific) according to the manufacturer's instructions. Global gene expression profiling was performed by GeneChip® Human Genome U133 Plus 2.0 arrays (Affymetrix), which provides comprehensive coverage for over 38,500 human genes. The microarray experiments and genome-wide expression quantification were carried out by the Case Western Reserve University Gene Expression Core. Raw intensities of 54,675 probes were quantified and normalized by the robust multi-array average (RMA) algorithm in the R package *affy*. Low-quality probes were filtered out using the *shorth* function built-in R package *genefilter*, and 32,406 probes remained for downstream analysis. Linear regression models were used to identify expression probes showing differential expression in *ANRIL* si*ANRIL*-treated cells compared with *siNC*-treated cells. An empirical Bayes method implemented in R package *limma* was applied to shrink the probe-wise sample variances toward a common value and to augment the degrees of freedom for the individual variances. To control the false discovery rate (FDR) in multiple testing, the q values were calculated using the Benjamini–Hochberg FDR procedure. Significant probes were defined as those with $q < 0.05$. The data discussed in this paper have been deposited in NCBI's Gene Expression Omnibus and are accessible through GEO Series accession number GSE117676.

Enrichment analysis of biological pathways

A gene set enrichment analysis tool, ClueGO version 2.3.3 (20), and public databases including GO, KEGG, and REACTOME were used to identify the biological processes or pathways enriched by *ANRIL* downstream genes. Significant pathways were further assigned into functional groups based on κ similarity scores of >0.60. The p values were calculated using a two-sided hypergeometric test and adjusted for multiple testing with Bonferroni correction.

Semi-quantitative RT-PCR analysis

Total RNA samples were isolated from the transfected cells as described above and reverse-transcribed into cDNA using random primers (Invitrogen). The cDNA was used for PCR analysis with primers specific for *ANRIL* downstream genes for different numbers of cycles. Primer sequences for individual genes are listed in Table S2. Each forward and reverse primer was designed to target different exons to avoid replication of the genomic DNA. The PCR products were analyzed using a 2% agarose gel. Each set of reactions always included a no-sample negative control.

Real-time RT-PCR analysis

Total RNA samples were isolated from the transfected cells as described above and converted into cDNA. The RT-PCR analysis was performed in a final volume of 20 μl containing 10 μl of Power SYBR Green PCR Master Mix kit (Applied Biosystems), 0.4 μl of each primer at 10 pmol/μl, and 2 μl of the cDNA solution using an Applied Biosystems Prism 7900HT (Applied Biosystems) system. The same primers from the semi-quantitative RT-PCR analysis (Table S2) were used in qRT-PCR analysis as well. Raw data were analyzed using Sequence Detection System (SDS) software version 2.4 (Applied Biosystems) and compared by the $\Delta\Delta Ct$ method as described previously by us (6, 13, 30–35). Results are expressed relative to the housekeeping GAPDH transcript quantity and normalized to untreated cells. Each sample was analyzed three times.

Western blot analysis

HCAECs were activated with 10 ng/ml TNFα for 15 min, washed twice with ice-cold PBS, and lysed using lysis buffer

containing 50 mmol/liter Tris, pH 7.8, 150 mmol/liter NaCl, 0.5% sodium deoxycholate, 1% Nonidet P-40, anti-protease, and anti-phosphatase. Protein concentrations were determined using the BCA protein assay kit (Bio-Rad). Lysates were loaded onto a 10% SDS-polyacrylamide gel for electrophoresis and then transferred onto Immobilon-P membranes (GE Healthcare). The membranes were incubated in 5% (w/v) BSA in TBS for 1 h and then further reacted with primary antibodies. The antibodies included rabbit anti-ICAM1 (1:1,000; Santa Cruz Biotechnology, Inc.), rabbit anti-ICAM2 (1:1,000; GTX), rabbit anti-VCAM1 (1:1,000; Cell Signaling), mouse anti-E-selectin (1:1,000; Santa Cruz Biotechnology), mouse anti-P-selectin (1:1,000; Santa Cruz Biotechnology), rabbit anti-VE-Cad total (1:1,000; Cell Signaling), rabbit anti-VE-Cad phospho-Ser-536 (1:1,000; Cell Signaling), mouse anti-GAPDH (1:1,000; Millipore), mouse anti-β-tubulin (1:1,000; Santa Cruz Biotechnology), rabbit anti-N-cadherin (1:1,000; Novus Biologicals), mouse anti-CLIP-170 (1:1,000; Cell Signaling), mouse anti-ezrin (1:1,000; Cell Signaling), and rabbit anti-LYVE-1 (1:1,000; Abcam). After extensive washes, the membranes were incubated with anti-rabbit or anti-mouse IR secondary antibodies, IRDye (1:10,000; LI-COR Biosciences). Protein bands were visualized using an Odyssey CLx imaging system (LI-COR Biosciences) and then analyzed using Image Studio version 5.2 and ImageJ software. Four independent experiments were performed.

Similar Western blot analysis was also performed with plasma membrane protein extracts isolated by biotinylation and NeutrAvidin pulldown with the EZ-Link Sulfo-NHS-SS-Biotin kit (Thermo Fisher Scientific) as described previously by us (15).

Statistical analysis

Data are presented as mean ± S.D. Statistical analysis was performed using Student's t test (paired and two-tailed) or using analysis of variance using GraphPad Prism version 7 software. $p < 0.05$ was used as a cut-off value to determine statistical significance of the data.

Author contributions—H. C., Q. C., and Q. K. W. designed the study; H. C., G. Q. S., X. W., F. W., S. A., Y. L., G. Y., S. C., Q. C., and Q. K. W. performed experiments and data analysis; H. C., Q. C., and Q. K. W. drafted the manuscript; all authors critically revised the manuscript; Q. C. and Q. K. W. supervised the project.

Acknowledgments—We thank Dr. Chun Fan for preparing samples for microarray analysis, Dr. Alpha S. Yap for CLIP1 expression plasmids, and Drs. Ahmad Khalil, Zhenghe Wang, and Hua Lou and all of the Wang laboratory members for discussion and advice.

References

1. Matsuzawa, Y., and Lerman, A. (2014) Endothelial dysfunction and coronary artery disease: assessment, prognosis, and treatment. *Coron. Artery Dis.* **25,** 713–724 CrossRef Medline
2. Libby, P. (2002) Inflammation in atherosclerosis. *Nature* **420,** 868–874 CrossRef Medline
3. Lessner, S. M., Prado, H. L., Waller, E. K., and Galis, Z. S. (2002) Atherosclerotic lesions grow through recruitment and proliferation of circulating monocytes in a murine model. *Am. J. Pathol.* **160,** 2145–2155 CrossRef Medline
4. Helgadottir, A., Thorleifsson, G., Manolescu, A., Gretarsdottir, S., Blondal, T., Jonasdottir, A., Jonasdottir, A., Sigurdsson, A., Baker, A., Palsson, A., Masson, G., Gudbjartsson, D. F., Magnusson, K. P., Andersen, K., Levey, A. I., *et al.* (2007) A common variant on chromosome 9p21 affects the risk of myocardial infarction. *Science* **316,** 1491–1493 CrossRef Medline
5. McPherson, R., Pertsemlidis, A., Kavaslar, N., Stewart, A., Roberts, R., Cox, D. R., Hinds, D. A., Pennacchio, L. A., Tybjaerg-Hansen, A., Folsom, A. R., Boerwinkle, E., Hobbs, H. H., and Cohen, J. C. (2007) A common allele on chromosome 9 associated with coronary heart disease. *Science* **316,** 1488–1491 CrossRef Medline
6. Cheng, X., Shi, L., Nie, S., Wang, F., Li, X., Xu, C., Wang, P., Yang, B., Li, Q., Pan, Z., Li, Y., Xia, H., Zheng, C., Ke, Y., Wu, Y., *et al.* (2011) The same chromosome 9p21.3 locus is associated with type 2 diabetes and coronary artery disease in a Chinese Han population. *Diabetes* **60,** 680–684 CrossRef Medline
7. Wang, F., Xu, C. Q., He, Q., Cai, J. P., Li, X. C., Wang, D., Xiong, X., Liao, Y. H., Zeng, Q. T., Yang, Y. Z., Cheng, X., Li, C., Yang, R., Wang, C. C., Wu, G., *et al.* (2011) Genome-wide association identifies a susceptibility locus for coronary artery disease in the Chinese Han population. *Nat. Genet.* **43,** 345–349 CrossRef Medline
8. Kong, Y., Sharma, R. B., Nwosu, B. U., and Alonso, L. C. (2016) Islet biology, the CDKN2A/B locus and type 2 diabetes risk. *Diabetologia* **59,** 1579–1593 CrossRef Medline
9. Holdt, L. M., Hoffmann, S., Sass, K., Langenberger, D., Scholz, M., Krohn, K., Finstermeier, K., Stahringer, A., Wilfert, W., Beutner, F., Gielen, S., Schuler, G., Gäbel, G., Bergert, H., Bechmann, I., *et al.* (2013) Alu elements in ANRIL non-coding RNA at chromosome 9p21 modulate atherogenic cell functions through trans-regulation of gene networks. *PLoS Genet.* **9,** e1003588 CrossRef Medline
10. Holdt, L. M., Beutner, F., Scholz, M., Gielen, S., Gäbel, G., Bergert, H., Schuler, G., Thiery, J., and Teupser, D. (2010) ANRIL expression is associated with atherosclerosis risk at chromosome 9p21. *Arterioscler. Thromb. Vasc. Biol.* **30,** 620–627 CrossRef Medline
11. Holdt, L. M., Sass, K., Gäbel, G., Bergert, H., Thiery, J., and Teupser, D. (2011) Expression of Chr9p21 genes CDKN2B (p15(INK4b)), CDKN2A (p16(INK4a), p14(ARF)) and MTAP in human atherosclerotic plaque. *Atherosclerosis* **214,** 264–270 CrossRef Medline
12. Archacki, S., and Wang, Q. (2004) Expression profiling of cardiovascular disease. *Hum. Genomics* **1,** 355–370 CrossRef Medline
13. Bai, Y., Nie, S., Jiang, G., Zhou, Y., Zhou, M., Zhao, Y., Li, S., Wang, F., Lv, Q., Huang, Y., Yang, Q., Li, Q., Li, Y., Xia, Y., Liu, Y., *et al.* (2014) Regulation of CARD8 expression by ANRIL and association of CARD8 single nucleotide polymorphism rs2043211 (p.C10X) with ischemic stroke. *Stroke* **45,** 383–388 CrossRef Medline
14. Holdt, L. M., and Teupser, D. (2012) Recent studies of the human chromosome 9p21 locus, which is associated with atherosclerosis in human populations. *Arterioscler. Thromb. Vasc. Biol.* **32,** 196–206 CrossRef Medline
15. Zhao, Y., Huang, Y., Li, W., Wang, Z., Zhan, S., Zhou, M., Yao, Y., Zeng, Z., Hou, Y., Chen, Q., Tu, X., Wang, Q. K., and Huang, Z. (2015) Post-transcriptional regulation of cardiac sodium channel gene SCN5A expression and function by miR-192–5p. *Biochim. Biophys. Acta* **1852,** 2024–2034 CrossRef Medline
16. Ridker, P. M., Everett, B. M., Thuren, T., MacFadyen, J. G., Chang, W. H., Ballantyne, C., Fonseca, F., Nicolau, J., Koenig, W., Anker, S. D., Kastelein, J. J. P., Cornel, J. H., Pais, P., Pella, D., Genest, J., *et al.* (2017) Antiinflammatory therapy with canakinumab for atherosclerotic disease. *N. Engl. J. Med.* **377,** 1119–1131 CrossRef Medline
17. Hu, W., Lu, H., Zhang, J., Fan, Y., Chang, Z., Liang, W., Wang, H., Zhu, T., Garcia-Barrio, M. T., Peng, D., Chen, Y. E., and Guo, Y. (2018) Kruppel-like factor 14, a coronary artery disease associated transcription factor, inhibits endothelial inflammation via NF-κB signaling pathway. *Atherosclerosis* **278,** 39–48 CrossRef Medline
18. Wessel, F., Winderlich, M., Holm, M., Frye, M., Rivera-Galdos, R., Vockel, M., Linnepe, R., Ipe, U., Stadtmann, A., Zarbock, A., Nottebaum, A. F., and Vestweber, D. (2014) Leukocyte extravasation and vascular permeability

are each controlled *in vivo* by different tyrosine residues of VE-cadherin. *Nat. Immunol.* **15,** 223–230 CrossRef Medline

19. Vestweber, D. (2015) How leukocytes cross the vascular endothelium. *Nat. Rev. Immunol.* **15,** 692–704 CrossRef Medline
20. Bindea, G., Mlecnik, B., Hackl, H., Charoentong, P., Tosolini, M., Kirilovsky, A., Fridman, W. H., Pagès, F., Trajanoski, Z., and Galon, J. (2009) ClueGO: a Cytoscape plug-in to decipher functionally grouped gene ontology and pathway annotation networks. *Bioinformatics* **25,** 1091–1093 CrossRef Medline
21. Sun, X., Li, F., Dong, B., Suo, S., Liu, M., Li, D., and Zhou, J. (2013) Regulation of tumor angiogenesis by the microtubule-binding protein CLIP-170. *Protein Cell* **4,** 266–276 CrossRef Medline
22. Xie, S., Dong, B., Sun, X., Tala, He, X., Zhou, J., Liu, M., and Li, D. (2014) Identification of a cytoplasmic linker protein as a potential target for neovascularization. *Atherosclerosis* **233,** 403–409 CrossRef Medline
23. Zhao, L. P., Huang, L., Tian, X., Liang, F. Q., Wei, J. C., Zhang, X., Li, S., and Zhang, Q. H. (2016) Knockdown of ezrin suppresses the migration and angiogenesis of human umbilical vein endothelial cells *in vitro*. *J. Huazhong Univ. Sci. Technolog. Med. Sci.* **36,** 243–248 CrossRef Medline
24. Rey-Gallardo, A., Tomlins, H., Joachim, J., Rahman, I., Kitscha, P., Frudd, K., Parsons, M., and Ivetic, A. (2018) Sequential binding of Ezrin and Moesin to L-selectin regulates monocyte protrusive behaviour during transmigration. *J. Cell Sci.* **131,** jcs215541 CrossRef Medline
25. Nishida-Fukuda, H., Araki, R., Shudou, M., Okazaki, H., Tomono, Y., Nakayama, H., Fukuda, S., Sakaue, T., Shirakata, Y., Sayama, K., Hashimoto, K., Detmar, M., Higashiyama, S., and Hirakawa, S. (2016) Ectodomain shedding of lymphatic vessel endothelial hyaluronan receptor 1 (LYVE-1) is induced by vascular endothelial growth factor A (VEGF-A). *J. Biol. Chem.* **291,** 10490–10500 CrossRef Medline
26. Johnson, L. A., Banerji, S., Lawrance, W., Gileadi, U., Prota, G., Holder, K. A., Roshorm, Y. M., Hanke, T., Cerundolo, V., Gale, N. W., and Jackson, D. G. (2017) Dendritic cells enter lymph vessels by hyaluronan-mediated docking to the endothelial receptor LYVE-1. *Nat. Immunol.* **18,** 762–770 CrossRef Medline
27. Lim, J. P., and Gleeson, P. A. (2011) Macropinocytosis: an endocytic pathway for internalising large gulps. *Immunol. Cell Biol.* **89,** 836–843 CrossRef Medline
28. D'Angelo, R., Aresta, S., Blangy, A., Del Maestro, L., Louvard, D., and Arpin, M. (2007) Interaction of ezrin with the novel guanine nucleotide exchange factor PLEKHG6 promotes RhoG-dependent apical cytoskeleton rearrangements in epithelial cells. *Mol. Biol. Cell* **18,** 4780–4793 CrossRef Medline
29. Zhou, X., Han, X., Wittfeldt, A., Sun, J., Liu, C., Wang, X., Gan, L. M., Cao, H., and Liang, Z. (2016) Long non-coding RNA ANRIL regulates inflammatory responses as a novel component of NF-κB pathway. *RNA Biol.* **13,** 98–108 CrossRef Medline
30. Zhang, T., Yao, Y., Wang, J., Li, Y., He, P., Pasupuleti, V., Hu, Z., Jia, X., Song, Q., Tian, X. L., Hu, C., Chen, Q., and Wang, Q. K. (2016) Haploinsufficiency of Klippel–Trenaunay syndrome gene Aggf1 inhibits developmental and pathological angiogenesis by inactivating PI3K and AKT and disrupts vascular integrity by activating VE-cadherin. *Hum. Mol. Genet.* **25,** 5094–5110 Medline
31. Fan, C., Chen, Q., and Wang, Q. K. (2009) Functional role of transcriptional factor TBX5 in pre-mRNA splicing and Holt-Oram syndrome via association with SC35. *J. Biol. Chem.* **284,** 25653–25663 CrossRef Medline
32. Luo, C., Wang, F., Qin, S., Chen, Q., and Wang, Q. K. (2016) Coronary artery disease susceptibility gene ADTRP regulates cell cycle progression, proliferation, and apoptosis by global gene expression regulation. *Physiol. Genomics* **48,** 554–564 CrossRef Medline
33. Luo, C., Wang, F., Ren, X., Ke, T., Xu, C., Tang, B., Qin, S., Yao, Y., Chen, Q., and Wang, Q. K. (2017) Identification of a molecular signaling gene-gene regulatory network between GWAS susceptibility genes ADTRP and MIA3/TANGO1 for coronary artery disease. *Biochim. Biophys. Acta Mol. Basis Dis.* **1863,** 1640–1653 CrossRef Medline
34. Ye, J., Yao, Y., Song, Q., Li, S., Hu, Z., Yu, Y., Hu, C., Da, X., Li, H., Chen, Q., and Wang, Q. K. (2016) Up-regulation of miR-95-3p in hepatocellular carcinoma promotes tumorigenesis by targeting p21 expression. *Sci. Rep.* **6,** 34034 CrossRef Medline
35. Luo, C., Pook, E., Tang, B., Zhang, W., Li, S., Leineweber, K., Cheung, S. H., Chen, Q., Bechem, M., Hu, J. S., Laux, V., and Wang, Q. K. (2017) Androgen inhibits key atherosclerotic processes by directly activating ADTRP transcription. *Biochim. Biophys. Acta Mol. Basis Dis.* **1863,** 2319–2332 CrossRef Medline